Progress in Oceanography 235 (2025) 103494

Contents lists available at ScienceDirect

Progress in Oceanography

journal homepage: www.elsevier.com/locate/pocean

Jet stream poleward migration leads to marine primary production decrease

Júlia Crespin [a,*], Jordi Solé [b,c,d], Miquel Canals [a,d,e,f]

[a] GRC Geociències Marines, Departament de Dinàmica de la Terra i de l'Oceà, Universitat de Barcelona, Spain
[b] Institut de Ciències del Mar (CSIC), Barcelona, Spain
[c] Centre de Recerca Ecològica i Aplicacions Forestals (CREAF), Cerdanyola del Vallès, Spain
[d] Càtedra d'Economia Blava Sostenible, Universitat de Barcelona, Spain
[e] Reial Acadèmia de Ciències i Arts de Barcelona (RACAB), Barcelona, Spain
[f] Institut d'Estudis Catalans (IEC), Secció de Ciències i Tecnologia, Barcelona, Spain

ARTICLE INFO

Keywords:
Jet Stream$_1$
Marine Primary Production$_2$
Atmosphere-Ocean Interactions$_3$
Climate Change$_4$
Climate Change Impacts$_5$

ABSTRACT

Jet Streams (JS) are powerful upper-tropospheric winds that significantly influence weather and climate. As anthropogenic climate change alters temperature gradients, subtropical JS are expected to shift poleward, which can have unforeseen consequences on midlatitude Earth systems. Here, we demonstrate, for the first time, the impact of the steady poleward migration of the Northern Hemisphere subtropical JS on Marine Primary Production (MPP). Using over two decades of data (2000–2023), we establish a direct relationship between the JS latitudinal position and MPP variability in the Northwestern Mediterranean Sea. The observed northward migration of approximately 75 km over the study period aligns with a consistent decline in chlorophyll concentrations, representing a 40 % reduction, with rates reaching up to −5% per year. This is attributed to the steady northward seasonal shift of the JS position, which drives changes in northern wind-stress and Ekman pumping, subsequently reducing upwelling occurrence and intensity. While the primary influence of JS position on MPP is seasonal, we demonstrate that its impact extends to non-seasonal components as well. Unlike other studies linking JS shifts to short-term wind stress variations and isolated upwelling events, our findings highlight a long-term impact on MPP. Our findings suggest that JS dynamics is a dominant driver of MPP variability in the Northwestern Mediterranean Sea and point to equivalent situations in other marine regions worldwide. The cascading effects of reduced MPP have the potential to significantly impact marine ecosystems and resources, with broader implications for fisheries and the carbon cycle.

1. Introduction

Jet streams (JSs) are strong meandering upper-troposphere fast air currents that play a pivotal role in shaping weather patterns and climate dynamics on both regional and global scales (Woollings et al., 2010). Two primary types of near-tropopause JSs exist: the polar jets, located 9–12 km above the sea surface and embedded in the Polar front; and the subtropical jets, which are positioned at the poleward edge of the Hadley cell, at 10–16 km altitude (Holton and Staley, 1973; Bluestein, 1993). These features are pivotal to the understanding of atmospheric circulation, as they influence global energy transfer and drive variability in weather systems and climate. Subtropical jets, in particular, exhibit significant variability in strength and position, with profound implications for midlatitude daily weather and long-term climate (Archer and Caldeira, 2008; Hudson, 1979; Barnes and James, 2015; Stendel, et al., 2021).

Due to the alteration of midlatitude meridional temperature gradients because of anthropogenic climate change (Vallis et al., 2015; Woolings et al., 2023), subtropical JSs are expected to shift poleward (Meehl et al., 2007; Woollings and Blackburn, 2012; Vallis et al., 2015; Williams, 2016; Woollings et al., 2023). These shifts can profoundly affect atmospheric circulation patterns, modulating storm tracks, precipitation regimes, and the hydrological cycle (Hudson, 1979). Moreover, they may intensify vertical wind shear and atmospheric turbulence in midlatitude zones (Lv et al., 2021), with potential downstream effects on atmosphere–ocean interactions. Understanding JS variability and assess its impacts on interconnected Earth systems, including oceanic and biological processes, remains a critical and underexplored frontier.

* Corresponding author.
E-mail address: jcrespin@ub.edu (J. Crespin).

https://doi.org/10.1016/j.pocean.2025.103494
Received 17 January 2025; Received in revised form 2 May 2025; Accepted 4 May 2025
Available online 8 May 2025
0079-6611/© 2025 The Author(s). Published by Elsevier Ltd. This is an open access article under the CC BY license (http://creativecommons.org/licenses/by/4.0/).

One factor linked to subtropical JS migration is the observed expansion and intensification of the Azores High (Asiri et al., 2020; Cresswell-Clay et al., 2022), a semipermanent anticyclone that governs wind patterns over the northeastern Atlantic and western Mediterranean (Davis et al., 1997; Webster, 2004). This expansion, especially over North Africa and the southern Mediterranean, has contributed to both the northward shift of the JS (Woollings et al., 2023) as well as a vertical displacement from 200 hPa to 250 hPa (Asiri et al., 2020). As the JS migrates, it alters the position and intensity of winds, which are the main drivers of coastal upwelling in many midlatitude marine systems (Bakun, 1990; Lenoir et al., 2020).

In the northwestern Mediterranean Sea, upwelling is driven by persistent northwesterly and northerly winds that induce offshore Ekman transport, facilitating the upwelling of nutrient-rich deep waters (Millot, 1979; Millot, 1990; Bakun & Agostini, 2001; Katara et al., 2008; Fraysse et al., 2014; Many et al., 2021). Therefore, the strength and frequency of these winds could be largely influenced by the latitudinal shifts of the JS. However, quantifying this contribution remains complex, as JS dynamics interact with other synoptic and mesoscale atmospheric features (Griffin & Martin, 2017; Fedorova et al., 2018; Asiri et al., 2020; Osman et al., 2021). While previous studies have linked JS variability to changes in upper-ocean dynamics and marine productivity (Bane et al, 2001; Bane et al, 2007; Checkley and Barth, 2009; Barth et al., 2007; Le et al., 2022), direct observational evidence linking JS shifts to upwelling in this region remains scarce. Moreover, there remains a significant gap in understanding the long-term impacts of these

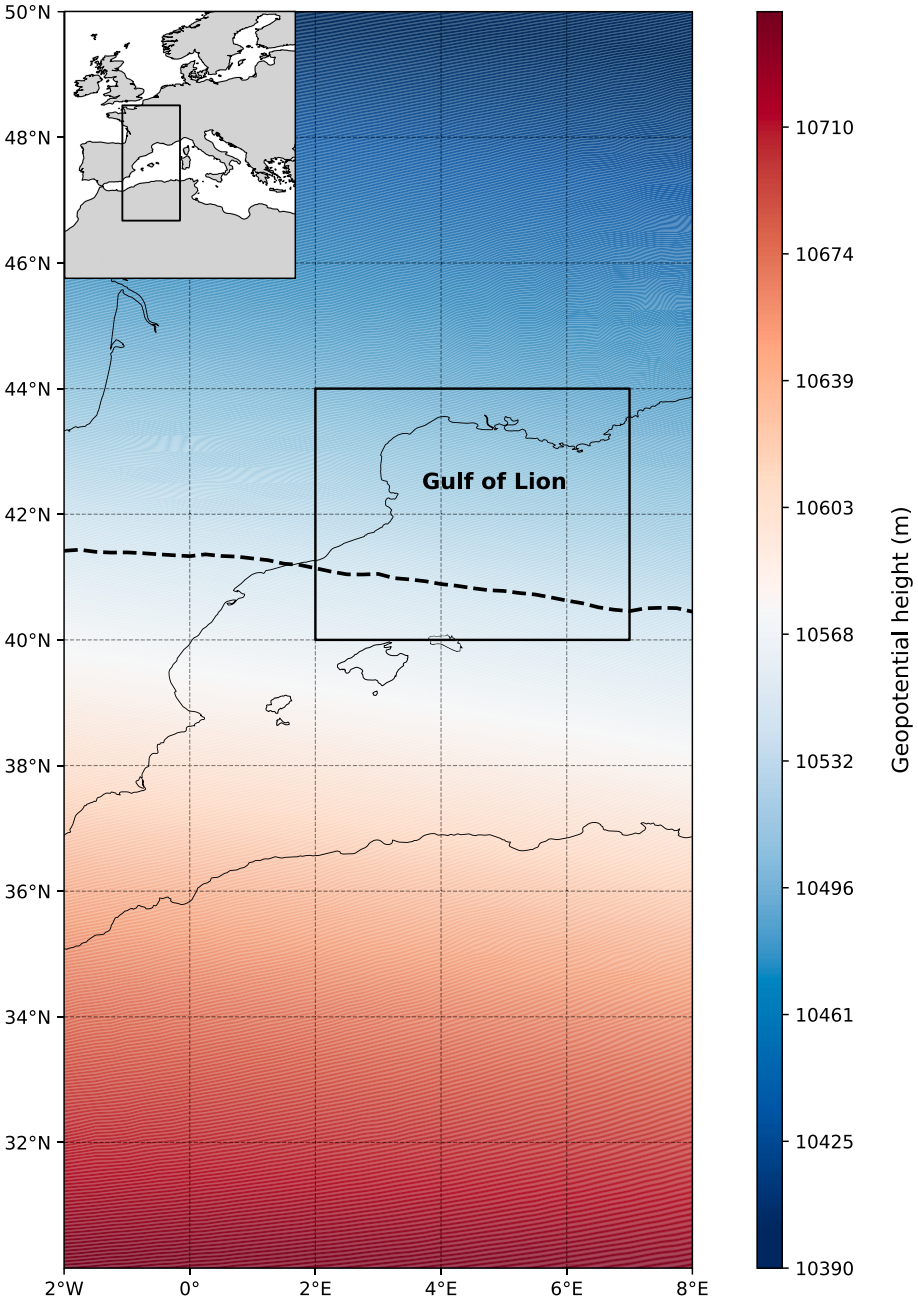

Fig. 1. Overall study domain, showing mean geopotential height (colour scale) from ERA5 reanalysis products on pressure levels, and the mean Jet Stream (JS) position (black dashed line) during the study period (2000–2023) (cf. Methods). JS position, northern wind stress, and Ekman pumping are calculated across the 32°–50°N latitudinal window along the central longitude of 4.0°E over the extended Gulf of Lion (black rectangle, 40°–44°N and 2°–7°E). Chlorophyll concentrations are averaged within the defined black square (cf. Materials and Methods).

shifts, particularly in the context of climate change.

Recent findings suggest that north–south shifts in the JS position can create a dipole effect in forest productivity and radial-growth anomalies across Europe (Dorado-Liñán et al., 2022; Xu et al., 2024). These findings suggest a broader atmospheric influence on primary production, underscoring the need to explore similar dynamics in marine ecosystems. In oceanic systems, JS variability may influence nutrient transport, wind-driven mixing, and upwelling; all vital for sustaining phytoplankton productivity (Gruber, 2011).

Our research aims to address these questions by examining the climatological position of the JS over a domain extending from central Europe to the western Mediterranean Sea and the adjacent North African landmass (32°–50°N; 2°W–8°E), and its impacts on the extended Gulf of Lion region (EGoL, 40°–44°N; 2°–7°E) (Fig. 1). This region is among the most productive areas in the Mediterranean Basin (Bosc et al., 2004; Bănaru et al., 2013; Stambler, 2014; Coll et al., 2024) and is characterized by intense atmosphere–ocean interactions, deep winter convection events, dense shelf water cascading, and frequent upwelling (Canals et al., 2006; Fourrier et al., 2022; Katara et al., 2008; Macias et al., 2018; Many et al., 2021; Mayot et al., 2017; Touratier et al., 2016; Keller et al., 2024; Renault et al, 2012; Tamburini et al, 2013). These features make it an ideal natural laboratory for investigating climate-driven atmospheric changes and their cascading effects on marine ecosystems. Furthermore, the recent documented decline in Marine Primary Production (MPP) in this region (Gómez-Jakobsen et al., 2022) highlights the urgency of identifying its underlying drivers, especially considering the Mediterranean's rapid warming trends and increasing variability (Hidalgo et al., 2022).

Using reanalysis and satellite-derived datasets, we investigate the links between JS position, wind forcing (northward wind stress, NWS), Ekman pumping (UPW), and chlorophyll concentration (CHL), a widely used proxy for MPP. Our analysis spans 2000–2024 and draws on ERA5 and Copernicus Marine Service reanalysis products. Further details are provided in the Materials and methods section. By analyzing atmosphere–ocean coupling mechanisms, we aim to assess whether JS migration contributes to the ongoing decline in MPP.

Through this work, we aim to enhance our understanding of the complex interactions between JS dynamics and marine productivity, ultimately contributing to the broader discourse on climate change impacts on marine ecosystems. By identifying key atmosphere–ocean coupling mechanisms, our findings could inform future climate adaptation strategies and marine resource management in the Mediterranean Sea and other midlatitude coastal regions.

2. Materials and Methods

2.2. Methodology

To investigate the potential relationship between JS position and MPP, we used a set of environmental and oceanographic variables, including geopotential Height (HGT) to determine the JS position, Northern Wind-Stress (NWS), Ekman pumping (UPW), satellite-derived chlorophyll concentrations (SAT-CHL), and depth-integrated chlorophyll concentrations (CHL) from reanalysis data. Chlorophyll concentrations serve as proxies for MPP, and we used two different types of chlorophyll data to capture both surface and depth-related processes. The choice of NWS and UPW was driven by their established role in modulating upwelling and oceanographic conditions that influence MPP, with chlorophyll being a key proxy for measuring primary productivity. The analysis was conducted using Python, with specific packages cited throughout.

The successive positions of the subtropical JS in the Northern Hemisphere were determined by computing the maximum HGT meridional gradient at 250 hPa, following the approach of Lv et al. (2021) over the 30°–50°N latitudinal range along the central longitude (4°E) of the EGoL region (Fig. 1). This methodology follows Bane et al (2001) and ensures that the jet's core is accurately located. The 250 hPa pressure level was chosen as it represents the altitude where the subtropical JS is most prominent, exhibiting the strongest wind speeds and clear gradients (Lv et al., 2021).

To assess the role of wind stress in oceanographic processes, we used wind components at 10 m above sea level (u_{10} and v_{10} components, representing zonal/eastward and meridional/northward winds, respectively) to compute the Northward Wind Stress (NWS), averaged over the same 30°–50°N latitudinal range (Fig. 1). The NWS was calculated using the following equations (1):

$$\tau_y = C_d \cdot \rho \cdot Ws \cdot v_{10} \quad (1)$$

where τ_y is the northern wind stress, ρ is air density (1.2 km·m^{-3}), C_d is the drag coefficient ($1.3 \cdot 10^{-3}$) (Taylor, 1916; Kalnay et al., 1996), and Ws is the wind speed, computed as (2):

$$Ws = \sqrt{{u_{10}}^2 + {v_{10}}^2} \quad (2)$$

This method quantifies the role of wind stress in driving oceanographic processes such as upwelling, which in turn impacts MPP.

Ekman pumping or upwelling (UPW), a proxy for upwelling strength, was computed following Smith (1988) (3):

$$W_{EK} = \frac{1}{\rho_{sw} f} \nabla \times \tau \quad (3)$$

where W_{EK} represents the Ekman upwelling velocity, ρ_{sw} is sea-water density (1025 kg·m^{-3}), f is the Coriolis parameter, and $\nabla \cdot \tau$ is the wind stress curl, calculated as (4):

$$\nabla \times \tau = \frac{\partial \tau_y}{\partial x} - \frac{\partial \tau_x}{\partial y} \quad (4)$$

where τ_x and τ_y are the zonal and meridional wind stress components, respectively.

UPW quantifies the vertical movement of water induced by wind stress curl (Von Schuckmann et al., 2019). While UPW is a primary driver of upwelling strength, other factors such as local bathymetry and water column stratification (Wang et al., 2013) can also influence upwelling, though they are not explicitly considered in this study.

Two types of chlorophyll data were used: surface chlorophyll concentrations (SAT-CHL) derived from multi-sensor satellite observations and depth-integrated Chlorophyll (CHL) concentrations from the Copernicus Marine Service Med Biogeochemistry reanalysis dataset. SAT-CHL provides insights into the immediate impact of surface processes such as light and nutrient availability on primary production. In contrast, the depth-integrated CHL, calculated from the surface to 60 m depth, includes deeper chlorophyll concentrations that are more relevant for assessing the overall productivity of the system, including subsurface dynamics that contribute to seasonal variations in primary production. The 60-meter depth level was chosen because it encompasses the mixed-layer depth and extends to a sufficient depth to account for the vertical distribution of phytoplankton and the dynamics of primary production throughout the water column, ensuring a more comprehensive representation of MPP throughout the year. The use of both surface and depth-integrated chlorophyll data allows for a more comprehensive assessment of MPP, capturing both immediate surface-level processes and deeper dynamics.

The time series of each variable were filtered to eliminate high-frequency variability using two different rolling window techniques following Bane et al, 2001 methodology. A primary 8-day rolling window was applied to the data to remove the weather-band noise and short-term variability that could obscure longer-term patterns in the data. Then, a secondary 35-day rolling window was also applied to capture the broader inter-annual variability by smoothing out short-term fluctuations. This window size was chosen because it allows for the extraction of meaningful trends that are not dominated by short-

term weather events or smaller cycles (such as weekly or bi-weekly patterns). The 8-day window was applied prior to the 35-day rolling window to ensure that short-term variations were adequately removed before evaluating longer-term trends.

The two windows were applied sequentially, with the shorter window first to address high-frequency noise and the longer window applied afterward to capture broader variability. This approach ensures that both small-scale and large-scale variability are properly accounted for in the analysis, providing a clearer understanding of the underlying patterns.

After filtering, we computed two-dimensional time-evolving means for each of the key variables (JS position, NWS, UPW, SAT-CHL, and CHL) to capture the variability in both temporal and spatial dimensions. The two dimensions refer to time (temporal evolution) and space (the variation across the variables and their respective geographical locations). These time-evolving means were calculated for each variable by averaging over time at each spatial location or depth level, allowing us to track how each variable evolves and interacts over the course of the study period.

Pearson correlations, p-values, and cross-correlations between the variables were calculated using the *scipy.stats.pearsonr* and *scipy.signal* functions from Scipy (Virtanen et al., 2020). These statistics were used to quantify the strength and significance of relationships among the variables.

Next, to determine the significant frequencies of the variables, we applied discrete Fast Fourier Transforms (FFT) using the *numpy.fft* function from Numpy (Harris et al., 2020). Temporal and spatial means, climatologies, variances, trends, and annual cycles were also calculated as preliminary statistics. Initially, trends were computed using the *numpy.polyfit* and *numpy.poly1d* functions also from Numpy (Harris et al., 2020). Subsequently, we applied the Mann-Kendall test to evaluate trends in our data. The Mann-Kendall test is a non-parametric statistical method designed to detect trends in time series data without the assumption of a specific distribution (Mann, 1945; Kendall, 1970). For this analysis, we utilized the pymannkendall library in Python (Hussain & Mahmud, 2019).

To remove both seasonal and long-term signals from the time series, we used the *seasonal_decompose* function from the *statsmodels.tsa.seasonal* library (Seabold & Perktold, 2010). This decomposition separates the time series into seasonal, trend, and residual components, allowing us to focus on the anomalies and underlying variability that are not explained by the seasonal cycle or long-term trends. The deseasonalization process was critical for isolating non-seasonal variations, particularly those related to inter-annual and decadal climate variability.

Principal Component Analysis (PCA) was applied to the correlation matrices of HGT, NWS, CHL, and UPW to identify dominant patterns of variability in these variables. This method reduces the dimensionality of the data while preserving the most significant modes of variability. FFTs were then applied to the obtained PCAs to identify their significant frequencies.

The variance patterns of JS position and CHL concentration beyond seasonal cyclicity were further investigated by means of an Empirical Orthogonal Functions (EOFs) analysis of the deseasoned and detrended HGT, NWS, and UPW time series. This method decomposes the data into independent modes (or dominant patterns) that are ranked according to the amount of variance in the dataset, therefore revealing underlying spatial structures within the relationships between different variables. EOFs and PCAs were performed using the *eofs* Python package (Dawson, 2016).

Additionally, to explore the causal relationships between the JS position and MPP (as represented by CHL concentration), we applied a convergent cross mapping causality test. This approach is grounded in the theory of non-linear dynamical systems and aims to distinguish genuine causal relationships from spurious correlations in time series data (Sugihara et al., 2012; Ye et al., 2015; Qing et al., 2023). The convergent cross mapping test works by examining whether the historical record of one variable (Y) can reliably predict the state of another variable (X) if the former is causally influencing the latter.

We implemented the tests' methodology using the *causal-ccm* Python package (Javier, 2021), which applies the method by estimating the optimal embedding dimension (E) and applying time lags (τ). We used an embedding dimension of 5 and a temporal lag of 20 days ($\tau = 20$), which were selected after testing various configurations to ensure robustness in the results. Both the original and the deseasonalized and detrended time series were analyzed to assess the causal relationships under different temporal conditions.

To assess the presence of significant temporal and spatial anomalies, we applied a rolling standard deviation (STD) analysis with a 35-day window to JS, SAT-CHL, and CHL to evaluate fluctuations and the extent of variability over time. The 35-day window was chosen because it captures medium-to-long-term fluctuations that are indicative of inter-annual variability, which is of particular interest in understanding the dynamics of the JS and MPP. This window allows for the identification of significant variability while smoothing out shorter-term noise.

For the calculation of anomalies, we used a reference period from January 1, 2000, to December 31, 2014, to compute both yearly and monthly anomalies. This reference period established the baseline climatology, with anomalies calculated as deviations from the mean for each corresponding month and year. Specifically, monthly anomalies were derived by subtracting the mean of each month (across the reference period) from the corresponding values in the time series. Similarly, yearly anomalies were calculated by subtracting the mean for each year (from the reference period) from the corresponding annual values in the dataset.

For spatial anomalies, we utilized Mediterranean Sea chlorophyll-a trend data from the Observations Reprocessing dataset (cf. 2.1 Data), based on multi-sensor satellite observations ('OMI_HEALTH_CHL_MEDSEA_OCEANCOLOUR_trend'). This dataset expresses trends as a percentage per year (% per year), representing relative changes compared to the reference climatology (1997–2014). Only statistically significant trends ($p < 0.05$) were included in this analysis.

The selection of reference periods for climatological anomalies follows a structured approach based on data availability and methodological consistency. For spatial trends, the reference period was constrained by the dataset provided by the Copernicus Marine Service, ensuring comparability with other studies and facilitating integration with global and regional climatological assessments.

To maintain methodological consistency for temporal anomalies, the reference period was defined using the full extent of our available dataset. Specifically, the depth-integrated CHL dataset spans from January 1, 2000, to May 31, 2023; the SAT-CHL covers the period from January 1, 2000, to December 2, 2024; and the JS position dataset extends from January 1, 2000, to December 9, 2024. This approach ensures a robust baseline climatology for temporal anomalies, reflecting the internal consistency of the dataset.

Thus, the difference in reference periods arises from the necessity to maintain internal consistency within our dataset for temporal anomalies while adhering to standardized datasets for spatial trends. This methodology ensures rigor while aligning with established climatological baselines used in oceanographic studies.

To evaluate broader atmospheric influences, a monthly time-series contour plot was created to highlight the seasonal cycle and intra-annual variability. To evaluate the broader atmospheric context, the North Atlantic Oscillation (NAO) (NCEI, 2023) and Western Mediterranean Oscillation (WeMO) (Martín-Vide and López-Bustins, 2006) indices were analyzed. While these indices are often linked to environmental variability in the NW Mediterranean Sea, no direct relationship was observed between these indices and the key variables in this study (Supp. Fig. 6).

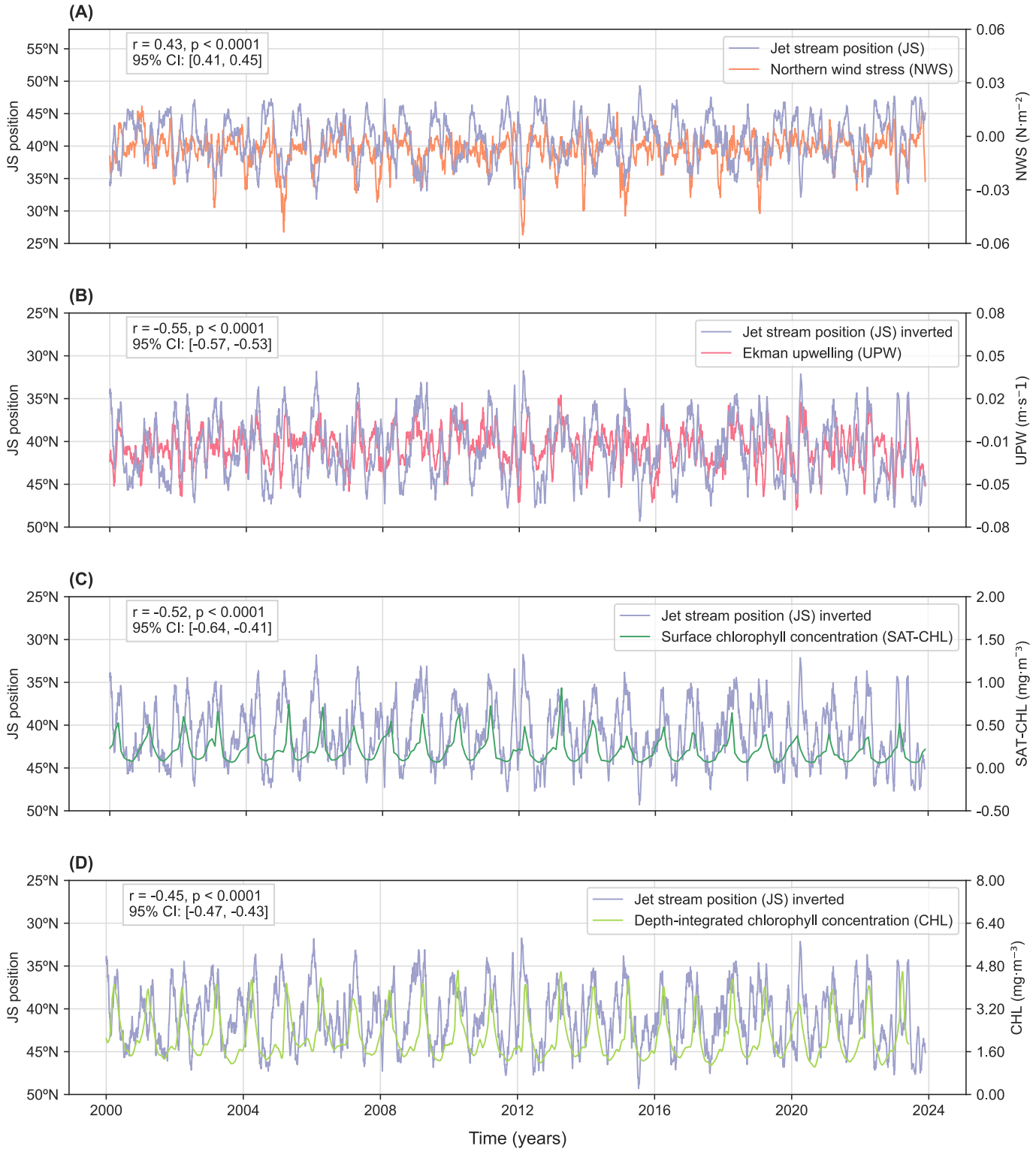

Fig. 2. Time-series of pairs of key variables showing their relationships for the 2000–2023 period. The plots show the JS position along 4°E against (A) Northern Wind Stress (NWS), (B) Ekman pumping (UPW), (C) monthly surface satellite-derived chlorophyll concentration (SAT-CHL), and (D) depth-integrated chlorophyll concentration (CHL). SAT-CHL and CHL are averaged across the extended Gulf of Lion (EGoL) subregion (black square in Fig. 1). Note that, in plots B, C and D, the JS position time-series are inverted to better illustrate the connection with its paired variable. Correlation coefficients (r), accompanied by their p-values (all $p < 0.0001$) and 95 % confidence intervals (CIs) within brackets, are shown in the upper left corner of all plots.

3. Results

3.1. Multidecadal connection between key variables and the jet stream

The time series of the above variables averaged across the EGoL subregion, along with their correlation coefficients (Fig. 2A–D), reveal that the JS position is negatively correlated with UPW (−0.55), surface chlorophyll concentration (SAT-CHL, r = -0.52), and depth-integrated CHL concentration (−0.45). Notably, all variables exhibit a pronounced seasonal cycle (Fig. 2A–D).

Given that depth-integrated CHL offers a more detailed representation of MPP by accounting for vertical integration, this dataset will serve as the primary focus of our analysis. SAT-CHL remains an essential complementary dataset to confirm that similar behavior and trends are likewise observed in satellite measurements, thereby enhancing the robustness of the results.

The deseasoned and detrended time series (cf. Methods) reveal key aspects of the relationship between JS position and MPP (Fig. 3A–C). The seasonal component, which reflects atmospheric dynamics and MPP processes, exhibits a strong inverse correlation (r = -0.80) (Fig. 3B). In contrast, the residual components of JS position and CHL concentration (deseasoned and detrended) show a weak but statistically significant positive correlation (r = 0.27, 95 % CI: 0.15–0.39) (Fig. 3C). This indicates that while the overall relationship beyond seasonal influences is limited, specific years show stronger coupling, as evident from visual inspection of certain time periods.

3.2. Yearly variability of coupling amongst variables

Building on the multidecadal relationship between JS position and MPP, we further examined the yearly variability of the coupling between JS position and key variables NWS, UPW, and CHL (Fig. 4). This analysis

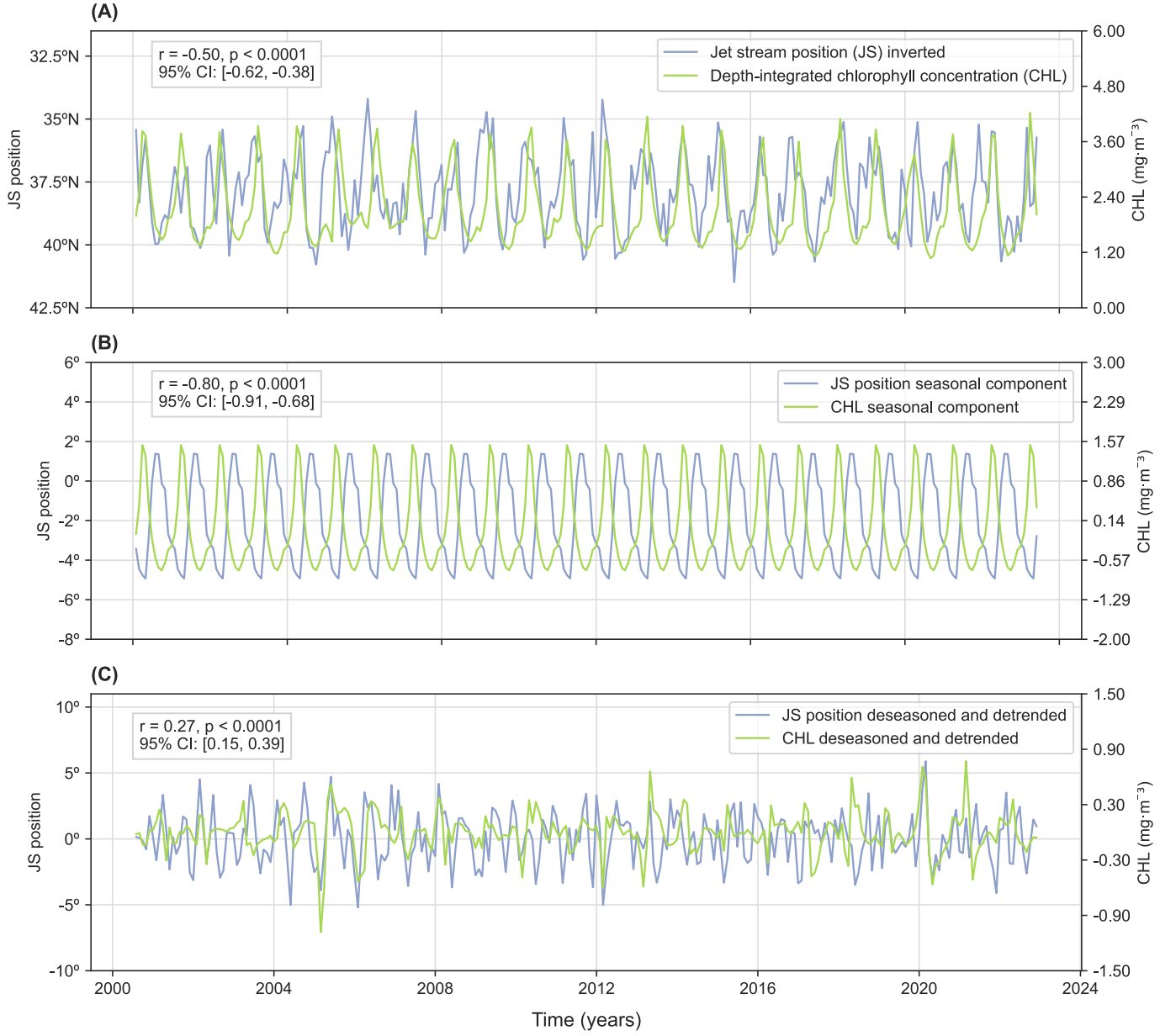

Fig. 3. Components of monthly Jet Stream (JS) position and Chlorophyll (CHL) time series for the study period from 2000 to 2023. (A) Monthly JS position (inverted) compared to monthly surface CHL concentration. (B) Seasonal components of the JS position and CHL time series, with interannual variability removed and trends detrended. (C) Residual components of the JS position and CHL time series after removing both seasonal and long-term trends. Correlation coefficients (r), along with their p-values (all $p < 0.0001$) and 95 % confidence intervals (CIs) in brackets, are displayed in the upper left corner of each plot.

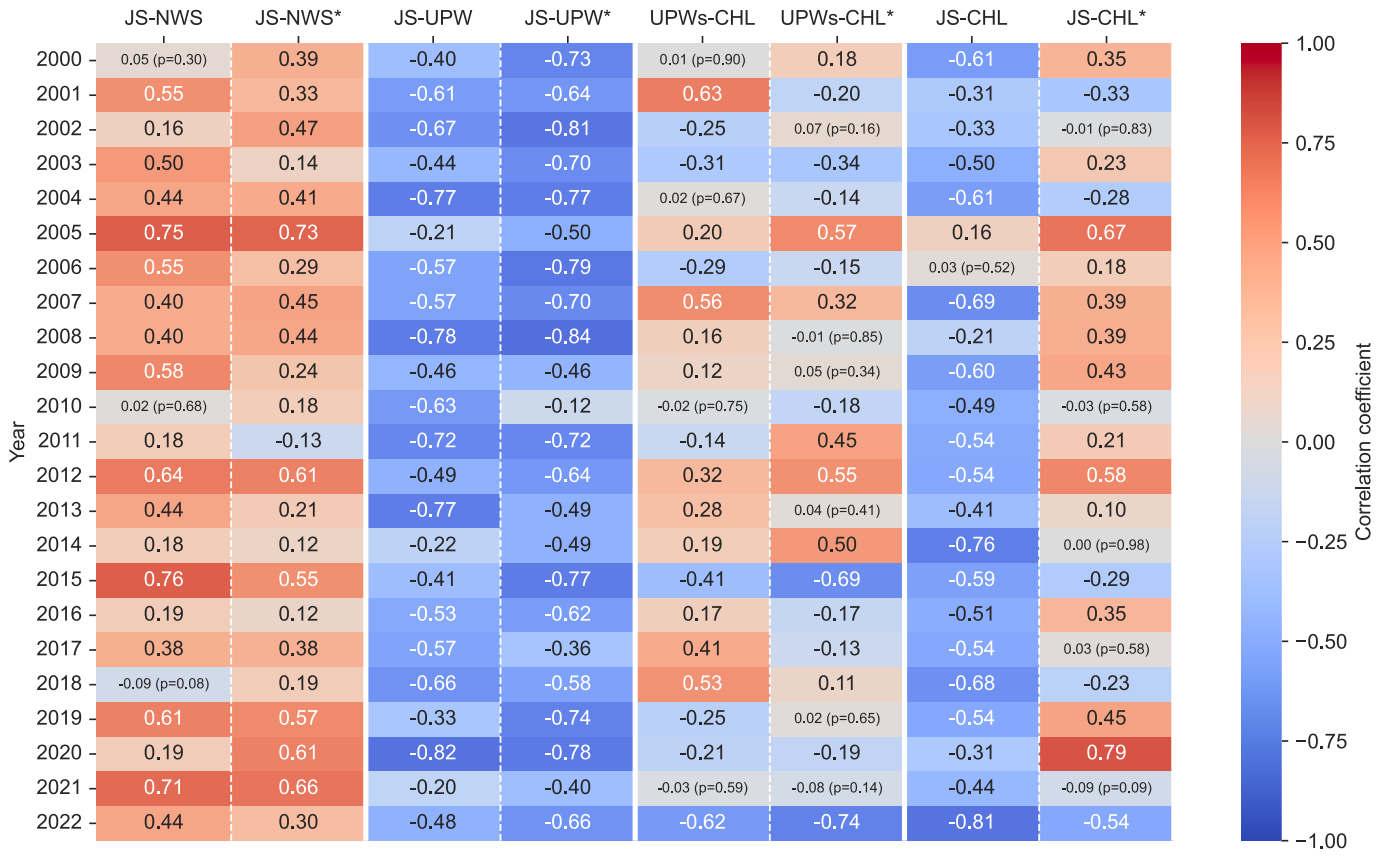

Fig. 4. Heatmap of annual correlation coefficients between variables from year 2000 to year 2022 using a "cool-warm" colour scale. Columns labelled with an asterisk (*) correspond to correlations between deseasoned and detrended variables. The higher the colour intensity, the stronger the positive (reddish) or negative (bluish) correlation amongst variables. Due to the availability of Copernicus Marine Service MED-BGC reanalysis chlorophyll data only until May 2023 (cf. Sect. 2), correlations were computed on an annual basis up to 2022. CHL: depth-integrated chlorophyll concentration. JS: jet stream position. NWS: northern wind stress. UPW: Ekman pumping or upwelling averaged across whole domain. UPWs: Ekman pumping or upwelling averaged across EGoL region. Correlation coefficients with non-significant p-values ($p > 0.05$) are annotated next to the corresponding values.

highlights how the strength of these relationships fluctuates year-to-year. Detrended and deseasonalized correlations are also shown for each variable (denoted with an asterisk). Correlation coefficients (r) are displayed in each cell, with p-values explicitly noted for non-significant correlations ($p > 0.05$).

The correlation between JS position and NWS remains consistently positive across the study period, with notably higher values in specific years. For example, strong positive correlations ($r \geq 0.7$) occur in 2005, 2015, and 2021, indicating robust coupling between the JS and NWS. Detrended and deseasonalized correlations (JS-NWS*) maintain a similar pattern, though with reduced magnitude in certain years (e.g., 2003, 2011, 2014, and 2016) (Fig. 4).

The inverse relationship between JS position and UPW is likewise consistent throughout the period, with the strongest negative correlations ($r \leq -0.7$) observed in years such as 2004, 2008, 2011, 2013, and 2020. In these years, the JS position appears to have a tightly coupled relationship with UPW. For detrended and deseasonalized data (JS-UPW*), the correlations follow a similar trend, with values more frequently exceeding $r = -0.70$, thus confirming the robustness of the inverse relationship even after the removal of seasonality and long-term trends.

When focusing on upwelling intensity averaged across the EGoL region (UPWs), relationships with CHL vary more substantially across years. While the raw UPWs–CHL correlation generally remains weak or insignificant, the detrended and deseasonalized UPWs–CHL* correlation reveals stronger patterns in certain years (e.g., 2005, 2012, 2014, 2015), suggesting that regional upwelling's influence on marine productivity becomes more apparent after adjusting for background variability.

The relationship between JS position and CHL also presents some variability depending on the years. Most years exhibit moderate to strong negative correlations (e.g., 2000, 2004, 2007, 2009, 2014, and 2018), but specific years show weaker correlations (e.g., 2005, 2008). Interestingly, the detrended and deseasonalized CHL correlations (JS-CHL*) highlight additional variability, with positive correlations in some years (e.g., 2005, 2012, and 2020) that contrast with the general negative relationship.

Year 2005 exhibits a strong coupling between JS and NWS, indicating an intensification of atmospheric control over wind stress dynamics. In this year, JS-UPW correlations are robust across both raw and deseasoned and detrended datasets. For JS-CHL, however, a strong positive correlation ($r = 0.67$) is observed, but only in the deseasoned and detrended data (JS-CHL*). In 2012, strong correlations are again evident, including a notable negative correlation for raw JS-CHL data ($r = -0.58$). Similarly, in 2015, a strong coupling is observed, but in this case with a negative coefficient for deseasoned and detrended UPWs-CHL and JS-CHL (UPWs-CHL* and JS-CHL*, repectively).

An additional pattern emerges between regional upwelling and chlorophyll variability. Years characterized by negative or weak correlations between UPWs–CHL* tend to coincide with negative correlations between JS–CHL*. These dynamics are particularly evident in years such as 2001, 2004, 2015, 2018, and 2022, where both JS–CHL* and UPWs–CHL* exhibit similarly low or negative values. Notably, these same years also exhibit weaker agreement between raw and deseasoned and detrended correlations of JS with NWS (e.g., lower JS–NWS and JS–NWS*), suggesting reduced coherence in atmospheric forcing across timescales.

An exception to this pattern is 2019, which shows a low UPWs–CHL* correlation but a very strong positive JS–CHL* correlation (r = 0.79). In that year, the raw JS–NWS correlation is weak (r = 0.19), but the deseasoned and detrended correlation is strong (JS-NWS*; r = 0.61), highlighting a case where short-term variability masks a more persistent underlying coupling between atmospheric dynamics and biological response.

Indeed, some years with stronger JS-NWS* correlations (e.g., 2005 and 2012) also show stronger JS-CHL* coefficients. Conversely, years with weak JS-UPW* correlations tend to exhibit similarly weak JS-CHL* coefficients, highlighting the influence of upwelling on MPP.

Years with non-significant correlations ($p > 0.05$) are clearly indicated in Fig. 4, reflecting periods of weaker coupling. For instance, JS-NWS correlations in 2000, 2010, and 2018 and JS-CHL* correlations in 2002, 2010, or 2021, show negligible or inconsistent patterns, emphasizing the year-specific nature of these relationships.

Together, these patterns highlight periods when JS variability is less tightly linked to both surface forcing and biological response across the EGoL region. This reinforces the idea that effective coupling between physical drivers and biological response is not always sustained, and that regional productivity can become decoupled from both upwelling intensity and jet positioning under certain atmospheric or oceanographic regimes.

3.3. Dominant frequencies and variance patterns

To further explore the temporal structure and underlying variability of the JS position and its connection to NWS, UPW, and CHL, Fast Fourier Transforms (FFTs) were applied to the time series of these variables. The results reveal highly similar spectra, with nearly identical dominant frequencies characterized by a clear intraseasonal oscillation or cyclicity of approximately 10–12 days (Fig. 5). This shared cyclicity indicates a coherent atmospheric forcing structure across the EGoL region.

In contrast, CHL spectrum only partially reflects this 10–12-day signal, suggesting that biological processes are influenced by, but not strictly coupled to, the high-frequency variability observed in JS, NWS, and UPW. The weaker or less distinct 10–12 day peak in CHL may result from integration of multiple physical drivers, biological buffering, or lags in response times that dampen high-frequency variability. This observation highlights more complex and temporally integrated nature of marine productivity compared to its physical drivers.

Time-lagged cross-correlation analysis between JS position and UPW, as well as between JS position and CHL concentration, highlights distinct time-response dynamics for the two variables (Fig. 6). For UPW, the strongest negative correlation occurs within a lag of 0 to 1 days (Fig. 6A), indicating a fast physical response to shifts in JS position. In contrast, CHL concentration exhibits the highest correlations at a lag of 15 to 40 days (Fig. 6B), reflecting a delayed biological response to JS oscillations.

Furthermore, the ~15–40 day delay in CHL response aligns well with the frequencies identified in the FFT analysis (Fig. 5), linking intraseasonal variability in JS positioning to productivity cycles in the EGoL. This supports the idea that short-term atmospheric fluctuations can imprint on marine ecosystems over longer timescales, modulated by the timing and efficiency of biological processes.

The first three EOFs modes for HGT, NWS, and UPW reveal the distinctive behavior of these variables in the entire Northwestern Mediterranean Sea, and particularly within the focus EGoL subregion (Fig. 7). Specifically, the maximum latitudinal gradient in the HGT EOFs, which represents the average deseasoned and detrended JS position for each mode, shows that in Mode 1 (55 % covariance), the JS crosses the EGoL subregion. In contrast, in Mode 3 (7 % covariance), the JS is located slightly southward, near the southern boundary of the EGoL (Fig. 7A).

For NWS (Fig. 7B), Mode 1 (50 % variance) and Mode 2 (19 % variance) clearly differentiate the EGoL subregion from the rest of the domain, with this distinction being particularly pronounced in Mode 2. Similarly, the EOF analysis of deseasoned and detrended UPW (Fig. 7C) reveals that 17 % (Mode 2) and 9 % (Mode 3) of the variance are concentrated along the EGoL coastaline, emphasizing localized upwelling patterns near the coastline.

To better understand how large-scale atmospheric pressure anomalies influence marine processes in the region, we performed a PCAs on

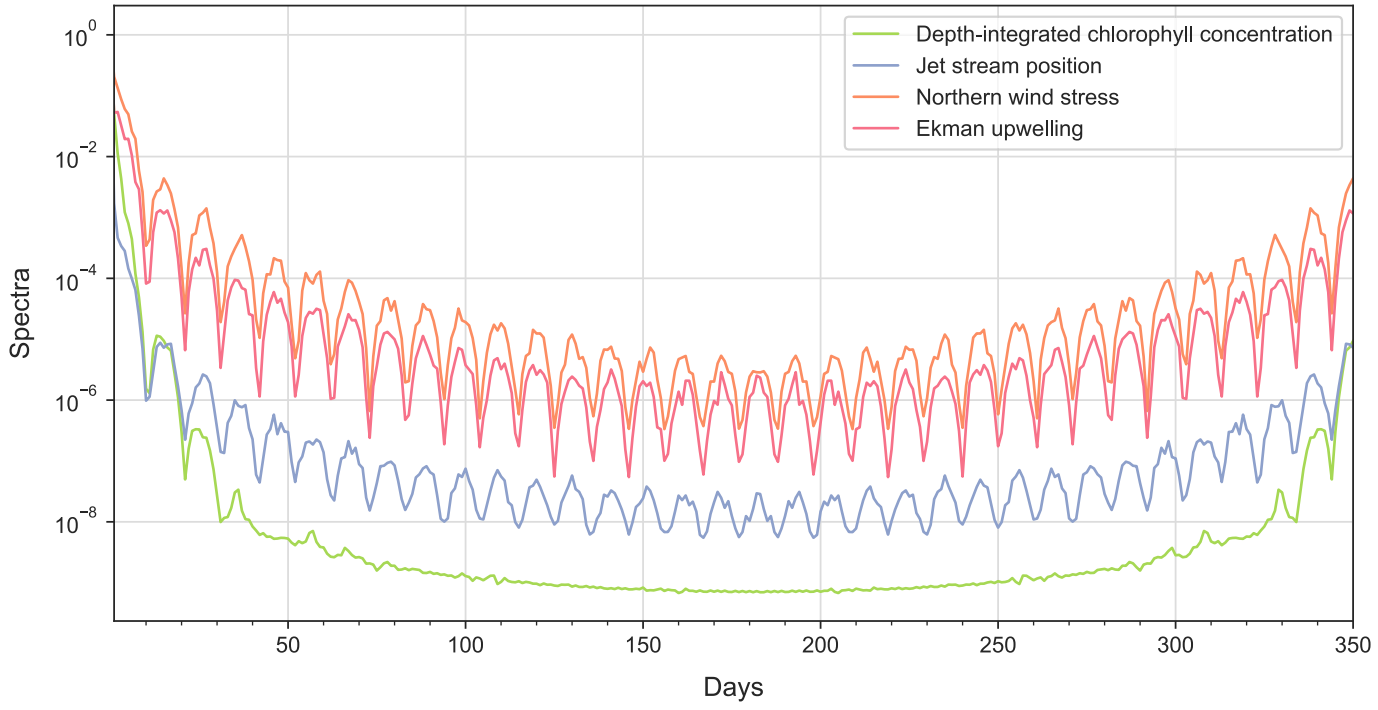

Fig. 5. Fast Fourier Transforms plot for depth-integrated chlorophyll concentration (green), jet stream position (blue), northern wind stress (orange), and Ekman upwelling (red). (For interpretation of the references to color in this figure legend, the reader is referred to the web version of this article.)

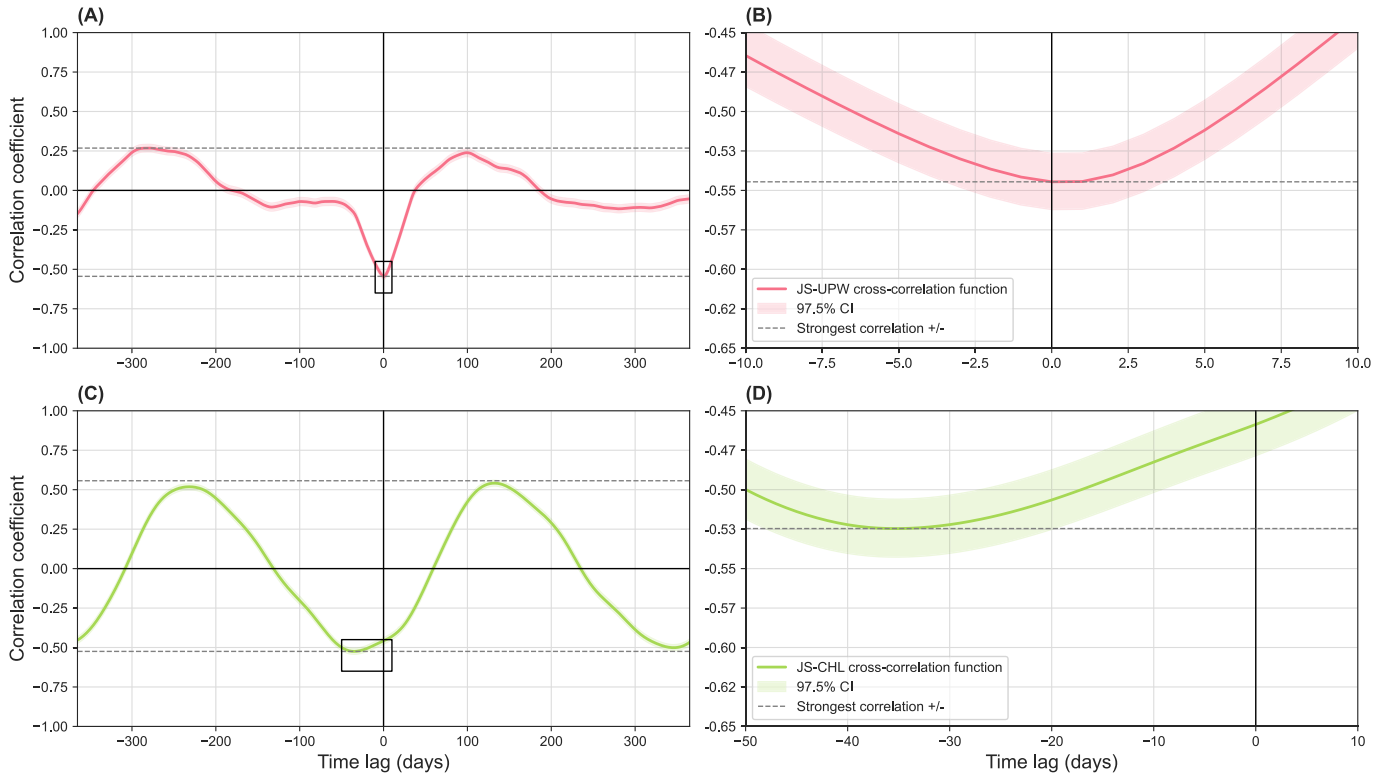

Fig. 6. Cross correlations between Jet Stream (JS) position, Ekman Upwelling (UPW) (red), and depth-integrated Chlorophyll (CHL) concentration (green), as a function of lag time (days). The left panel provides an overview, with the black square highlighting the zoomed area displayed in the right panel. The top row corresponds to JS-UPW cross-correlations (A-B), while the bottom row corresponds to JS-CHL cross-correlations (C-D). Horizontal grey dashed lines indicate the thresholds for the strongest positive and negative correlations, while the shaded areas in red and green represent the 97.5% confidence intervals (CI). The plots illustrate how the correlation coefficients (y-axis) between the variables evolve with varying lag days (x-axis). (For interpretation of the references to color in this figure legend, the reader is referred to the web version of this article.)

the monthly averaged HGT and compared it with monthly CHL and UPW anomalies. For CHL, the first PCA mode (Fig. 8A) shows a moderate positive correlation with HGT ($r = 0.53$, $p < 0.0001$), indicating that the dominant mode of atmospheric variability is linked to CHL fluctuations, likely through seasonal-scale synoptic forcing. The second mode shows a weaker but statistically significant negative correlation ($r = –0.14$, $p < 0.05$), while the third is not significant ($r = –0.03$, $p > 0.05$) (Fig. 8B–C). These findings are supported by FFT-based spectral correlation of the PCA modes (Supp. Fig. 1A), where Mode 1 shows a strong match in frequency content ($r = 0.94$, $p < 0.0001$), further reinforcing the connection between seasonal atmospheric dynamics and surface CHL variability. A moderate correlation ($r = 0.43$, $p < 0.0001$) is also observed for the second mode (Supp. Fig. 1B), and a weak correlation for the third mode ($r = 0.24$, $p > 0.05$) (Supp. Fig. 1C).

For UPW, we observe a similarly strong correlation between the first PCA mode of HGT and monthly averaged UPW ($r = 0.70$, $p < 0.0001$; Fig. 9A), highlighting the role of atmospheric pressure gradients and wind forcing in modulating coastal upwelling. Mode 2 shows no significant relationship ($r = 0.02$, $p > 0.05$), while Mode 3 is weakly but significantly correlated ($r = 0.19$, $p = 0.0012$; Fig. 9B–C). FFT analysis again confirms these relationships, with the highest spectral coherence for Mode 1 ($r = 0.99$, $p < 0.0001$), and moderate correlations for Modes 2 and 3 ($r = 0.32$ and $r = 0.36$, respectively; Supp. Fig. 2).

Together, these results demonstrate that seasonal to sub-seasonal atmospheric patterns, tightly linked to the JS variability, have a measurable influence on both upwelling and MPP in the study region.

3.4. Convergent cross mapping causality test

To assess the causal relationship between JS position and depth-integrated CHL, we employed the convergent cross mapping causality test. This analysis was conducted on both the original data (Fig. 10A–B) and the deseasoned and detrended data (Fig. 10C–D) to ensure that the observed relationship extended beyond seasonal components.

The results consistently show strong correlation coefficients, supporting a robust causal link between JS position and CHL concentration. The first column of Fig. 10 (panels A and C) presents the test results for the full time series, while panels B and D display results for the half time series. Notably, the causality strength coefficient (r) remains consistently high across all cases, with statistically significant p-values (<0.001). For both full and deseasoned data, correlation coefficients exceed 0.98, reinforcing the reliability of the causal relationship. Interestingly, when analyzing only half of the time series, the correlation is even higher, likely due to reduced variability or noise in shorter subsets of the 20-year dataset.

To further validate these findings, we conducted additional tests, summarized in Table S1. These explored different time series lengths (L) and various time lags (τ, in days). Across all cases, the highest correlations consistently emerged around a 20-day lag, coherent with Fig. 5, and the causality remained exceptionally strong ($r > 0.95$) for all tested time series lengths.

3.5. Temporal trends and anomalies

After examining the multidecadal connections (cf. Sect. 3.1), the year-to-year variability (cf. Sect. 3.2), dominant frequencies and variance patterns (cf. Sect. 3.3), and causality relationships (cf. Sect. 3.4), we now analyze their long-term temporal trends and anomalies to contextualize the observed variability within overarching trends and assess the cumulative changes over the study period.

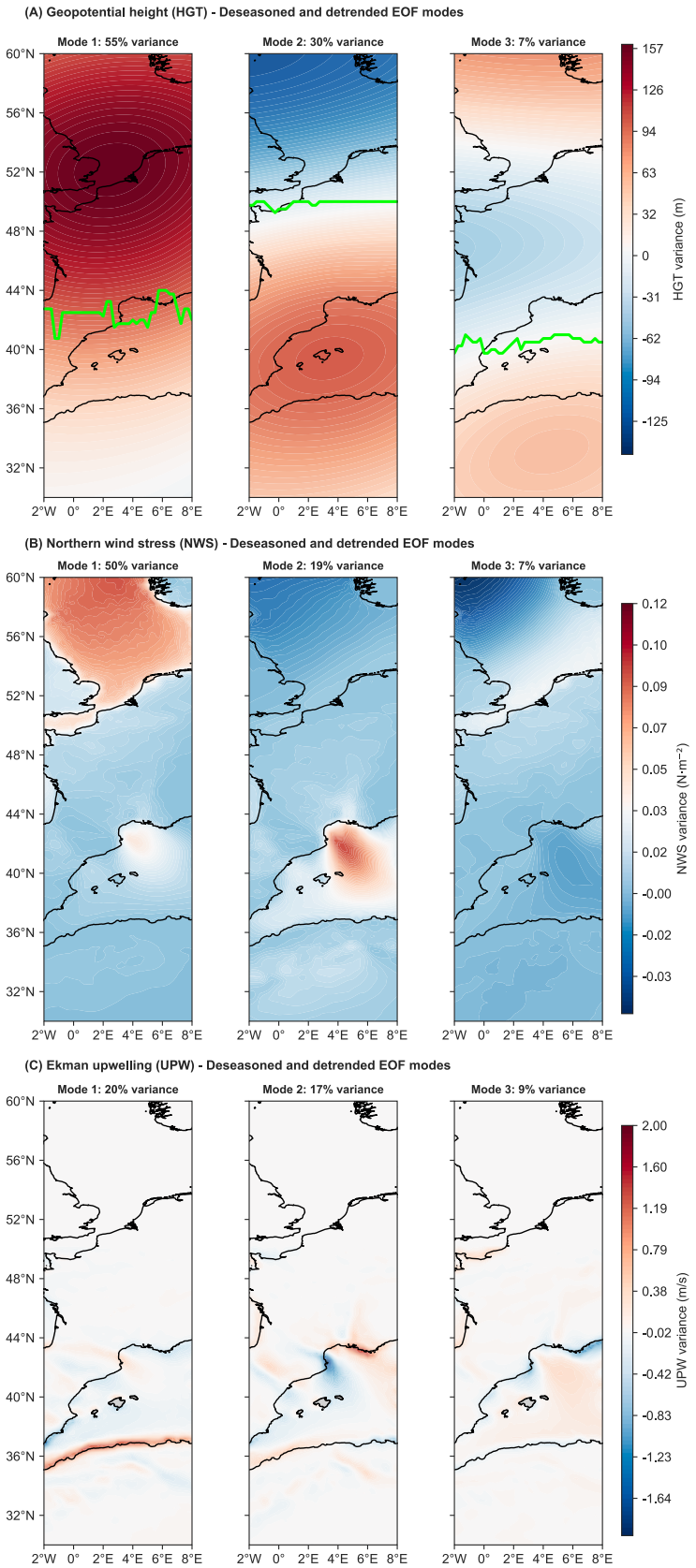

Fig. 7. The first three Empirical Orthogonal Functions (EOFs) modes for each variable, presented in three rows corresponding to (A) geopotential Height (HGT), (B) Northern Wind Stress (NWS), and (C) Ekman upwelling, based on deseasoned and detrended data across the study domain (refer to Fig. 1). Each row displays the first three EOF modes for the respective variable, with the percentage of covariance explained by each mode indicated above the plots. In panel (A), the thick lime green lines represent the location of the maximum HGT gradient for each EOF mode, which corresponds to the mean jet stream position. (For interpretation of the references to color in this figure legend, the reader is referred to the web version of this article.)

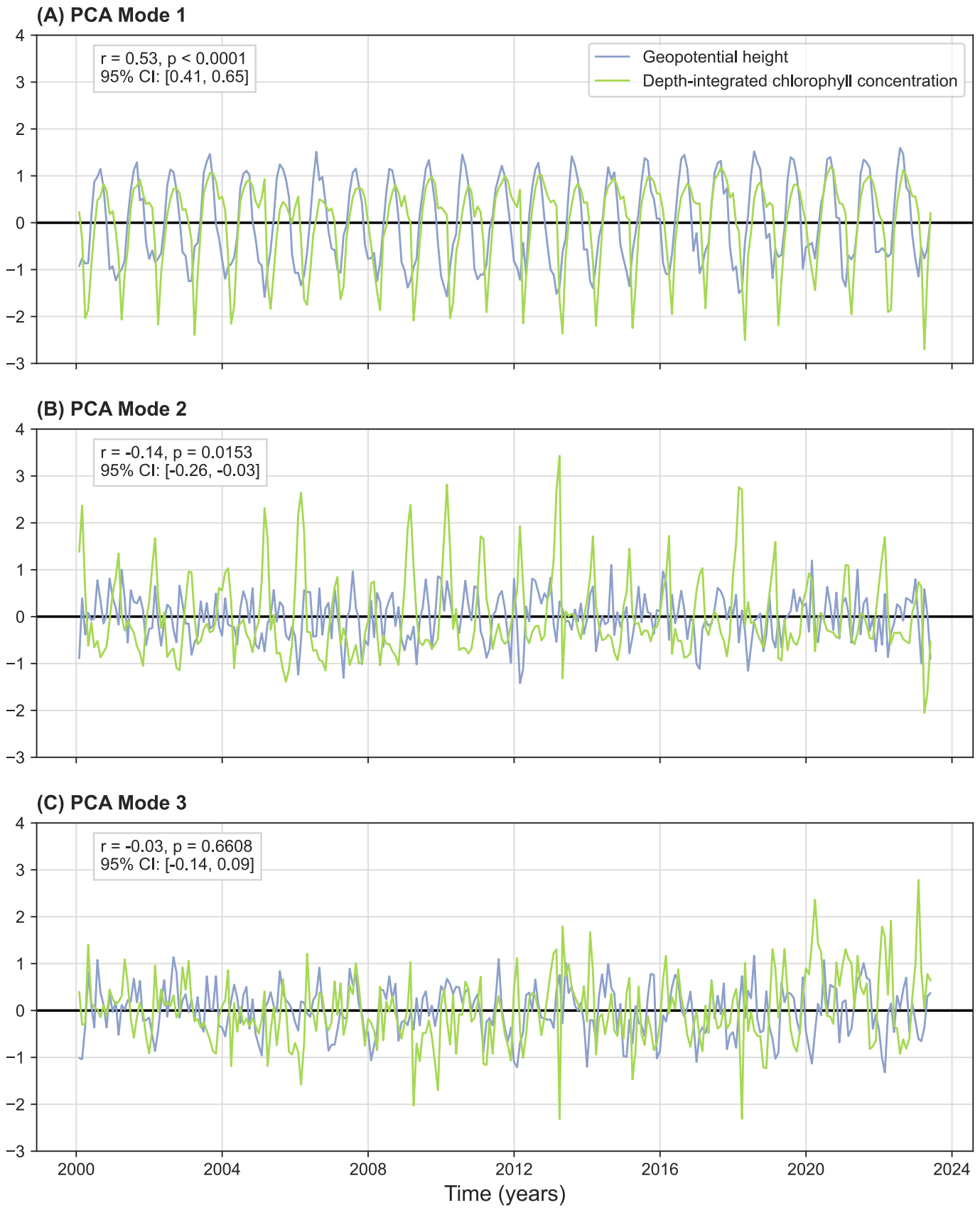

Fig. 8. Principal Component Analysis (PCA) for monthly geopotential height and monthly chlorophyll concentration. PCA modes 1, 2 and 3 (A, B and C, respectively) are illustrated. Correlation coefficients (r), accompanied by their p-values and 95% confidence intervals (CIs) within brackets, are shown in the upper left corner of all plots.

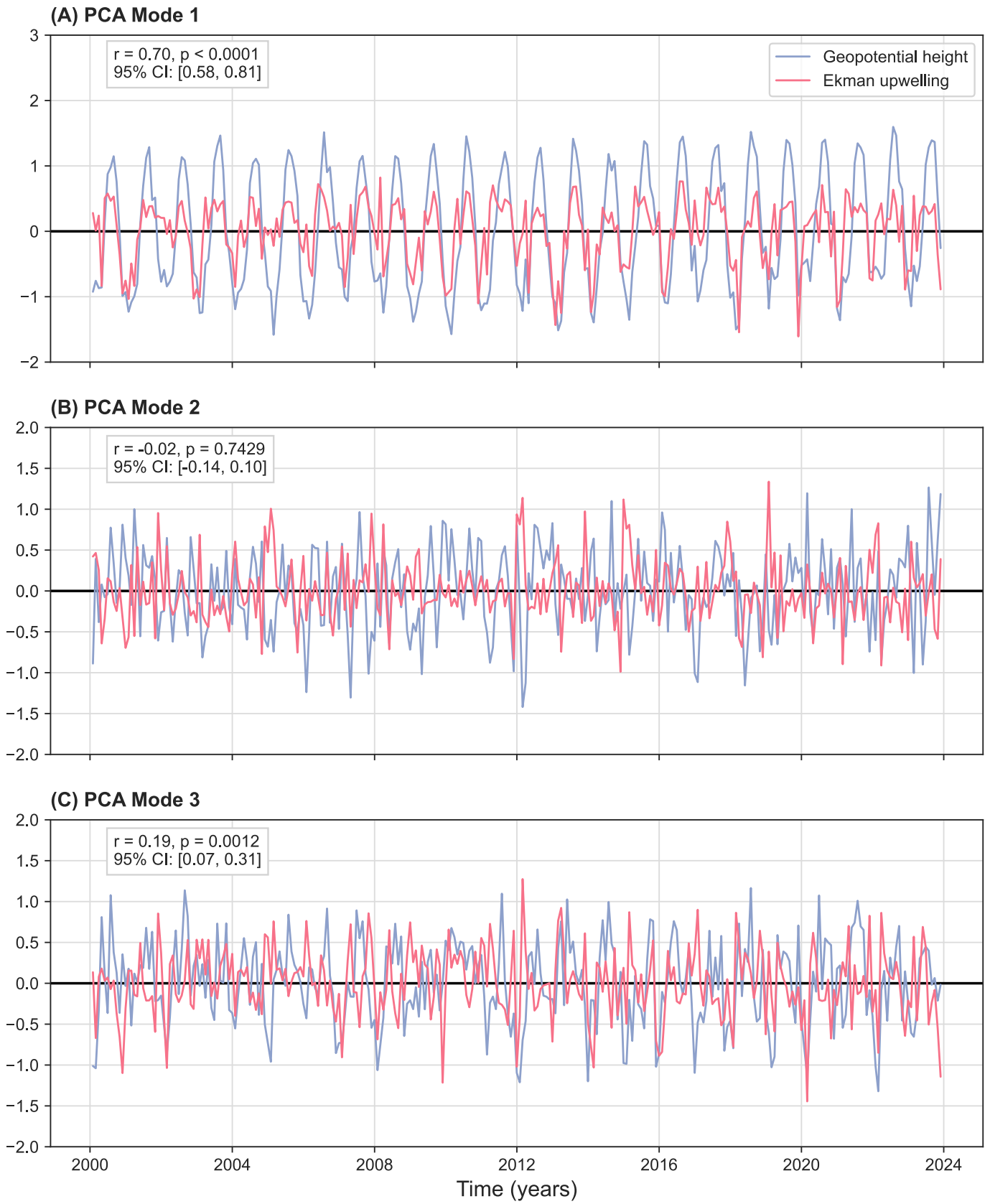

Fig. 9. Principal Component Analysis (PCA) for monthly geopotential height and monthly Ekman Upwelling (UPW). PCA modes 1, 2 and 3 (A, B and C, respectively) are illustrated. Correlation coefficients (r), accompanied by their p-values and 95% confidence intervals (CIs) within brackets, are shown in the upper left corner of all plots.

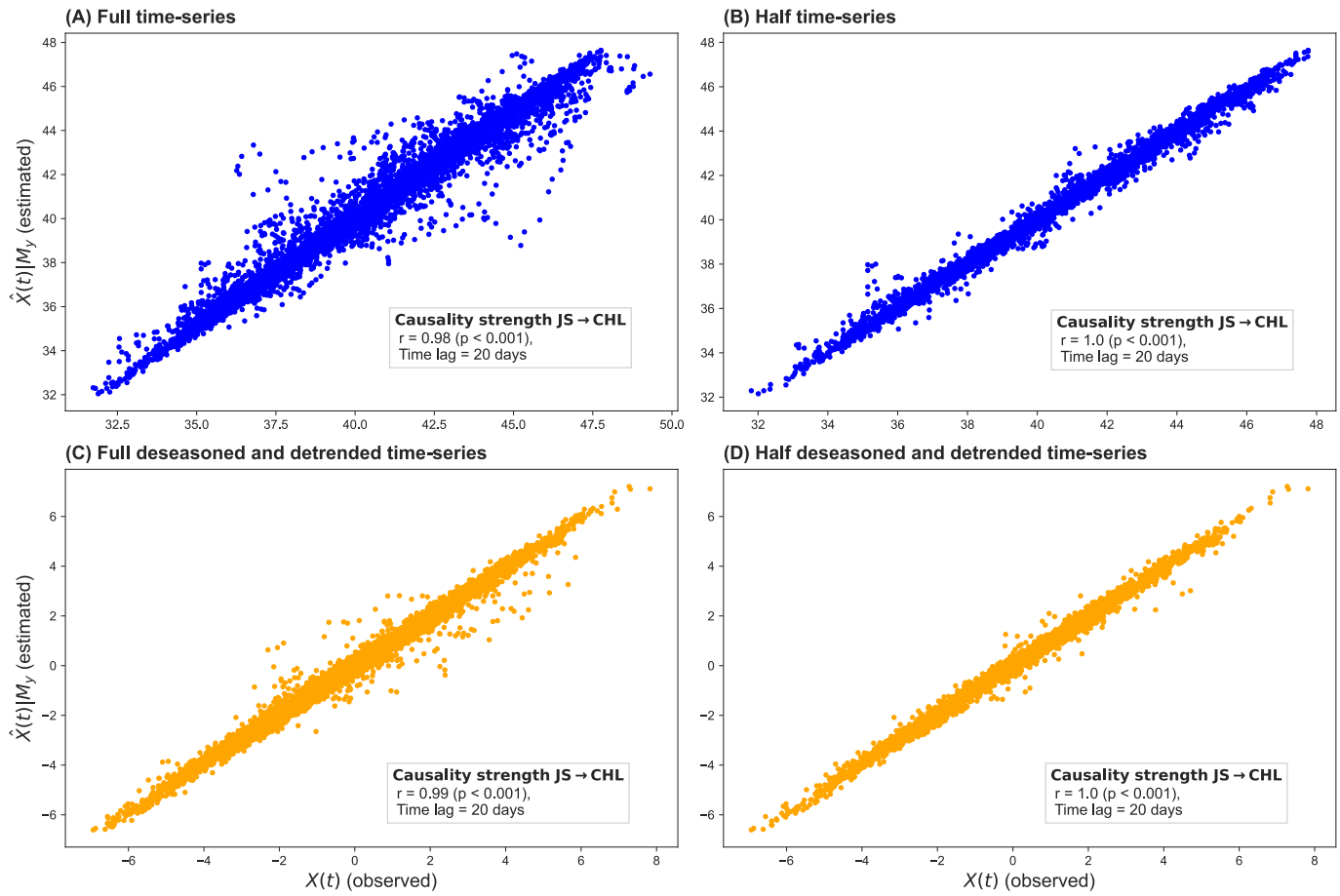

Fig. 10. Causality test results from the convergent cross mapping analysis between Jet Stream (JS) position and depth-integrated chlorophyll concentration (CHL). Panels (A) and (B) display results for the original time series, while panels (C) and (D) present results for the deseasoned and detrended data. The first column (A, C) shows the full time series, and the second column (B, D) focuses on the half time series. Each plot includes the correlation coefficient (r) and corresponding p-values ($p < 0.001$) in the lower right corner, along with the time lag (in days) applied during the analysis.

To this end, Mann-Kendall trend tests were applied to the full time series of key oceanographic and atmospheric variables. The JS latitudinal position exhibited a statistically significant increasing trend ($\tau = 0.036$, $p < 0.001$; Fig. 11A), indicating a gradual northward migration over the past two decades. Both surface chlorophyll (SAT-CHL; $\tau = -0.132$, $p < 0.001$) and depth-integrated CHL (CM; $\tau = -0.069$, $p < 0.001$) showed significant decreasing trends, suggesting a sustained reduction in marine productivity in the region (Fig. 11C–D). Upwelling intensity (UPW) also declined ($\tau = -0.024$, $p < 0.001$), although the magnitude of this change is relatively small (Fig. 11E). Conversely, the NWS displayed a statistically significant increasing trend ($\tau = 0.035$, $p < 0.001$; Fig. 11B), potentially reflecting shifts in regional wind dynamics, albeit with a similarly small effect. Full Mann-Kendall test statistics, including slope estimates, trend classification, and z-values, are provided in Supplementary Table 2.

A key finding from our analysis is the stark contrast in the trends of JS position and CHL concentration over the investigated period. Despite notable interannual variability (cf. Sect. 3.2), the JS shows a consistent northward displacement, amounting to approximately 75 km over the study period (Fig. 11A). In contrast, chlorophyll concentrations exhibit a steady decline throughout the EGoL subregion (Fig. 11C–D). This decline is evident in both depth-integrated CHL for the upper 60 m of the water column (Fig. 11C) and surface satellite-derived chlorophyll concentrations (Fig. 11D).

While the magnitude of the CHL decline seems relatively small, its significance becomes evident when contextualized within the climatological CHL concentrations and ecosystem productivity (Supp. Fig. 3). Specifically, for measured SAT-CHL, the trend reveals a reduction from ~0.21 to ~0.15 mg·m^{-3}, representing a ~30 % reduction over two decades. Although the absolute concentrations are relatively low, this substantial relative decline highlights a significant shift in MPP and ecosystem dynamics. Furthermore, spatial trends indicate a consistent negative pattern in CHL concentrations, with rates of decline reaching up to −5% per year Supp. Fig. 4), thus reinforcing the broad-scale impact of JS migration on MPP.

Additionally, we observe a clear tendency of yearly positive anomalies in the JS position over the investigated period, particularly in the last nine years, where almost all years exhibit positive anomalies (Fig. 12A). In the most recent two years, these anomalies approached nearly 1.5 latitudinal degrees (Fig. 12A). Notably, the two exceptions – 2018 and 2021 – are years where no significant correlations were found between JS position and CHL (Fig. 4), indicating a decoupling of the two variables during these years. In contrast, observed SAT-CHL anomalies reveal an even stronger negative trend over the same period (Fig. 12B), aligning with the overall decline in MPP identified throughout the study.

When analyzing monthly anomalies (Supp. Fig. 5), long-term patterns are less evident due to higher variability. However, two notable features emerge: (i) a high frequency of positive JS anomalies, especially in the last decade, and (ii) the occurrence of the two largest positive anomalies – exceeding 6° latitude – within the last five years of the study period (Supp. Fig. 5A). In contrast, measured SAT-CHL anomalies (Supp. Fig. 5B) show a clear negative tendency over the past eight years, reinforcing the observed decline in MPP and its connection to atmospheric forcing.

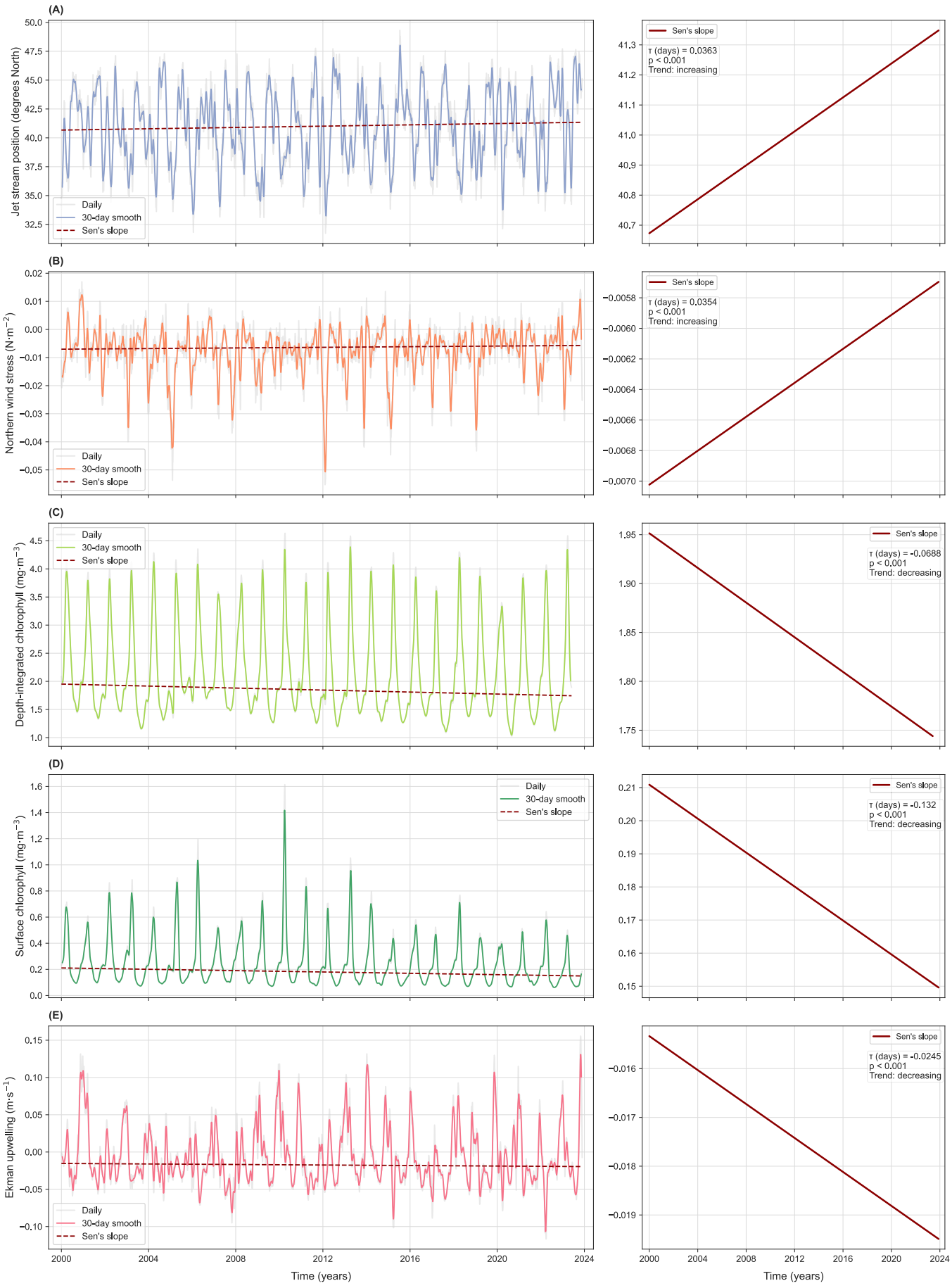

(caption on next page)

Fig. 11. Mann-Kendall results of Jet Stream (JS) position, Northern Wind Stress (NWS), depth-integrated chlorophyll concentration (CHL), satellite-derived surface chlorophyll (SAT-CHL), and Ekman Upwelling (UPW) averaged across the EGoL, with daily time series shown in light gray alongside their corresponding 30-day smoothed values in color. The general trends are indicated by Sen's slope (red lines) derived from the Mann-Kendall test across all panels. Panel (A) presents the JS position, panel (B) shows the NWS, panel (C) displays the CHL, panel (D) illustrates the SAT-CHL, and panel (E) depicts the UPW. The horizontal scale in the left plots is expanded to visualize seasonal (intra-annual) and interannual variability, while the right plots feature a compressed scale to highlight trends within the reference period (2000–2024). The right column also shows the details of the Mann-Kendall test results, including tau (τ), p-value, and whether the trend is increasing or decreasing. (For interpretation of the references to color in this figure legend, the reader is referred to the web version of this article.)

The statistical analysis of rolling standard deviations (STDs) for key atmospheric and oceanographic variables provides further insight into changes in interannual variability over the study period (2000–2024) (Supp. Fig. 6A). Notably, the JS position exhibits a significant and pronounced increasing trend in variability ($\tau = 0.054$, $p < 0.001$), with its rolling STD rising from approximately 1.05 to 1.22 degrees latitude over two decades (Supp. Fig. 6A). This indicates an increase in the variability of the JS latitudinal position, consistent with the observed frequency and magnitude of positive, but also negative anomalies in monthly JS position (Supp. Fig. 5A).

In contrast, the rolling STD of the NWS displays a significant decreasing trend ($\tau = -0.029$, $p < 0.001$), indicating slightly reduced variability in wind stress over time (Supp. Fig. 6B). SAT-CHL also shows a stronger significant decrease in variability ($\tau = -0.081$, $p < 0.001$), reinforcing the interpretation of a gradual and persistent decline in surface chlorophyll concentration rather than increasing episodic fluctuations (Supp. Fig. 6D). This pattern is further supported by the strongly negative trend in monthly SAT-CHL anomalies over the past eight years (Supp. Fig. 5B) and the smooth trajectory observed in yearly anomalies (Fig. 12B).

No significant trends were observed in the rolling STD of depth-integrated CHL ($\tau = 0.002$, $p = 0.772$) or upwelling intensity ($\tau = 0.014$, $p = 0.053$) (Supp. Fig. 6C, E), suggesting that the long-term decline in integrated chlorophyll and the modest reduction in upwelling intensity are not accompanied by systematic changes in their variability. Full Mann-Kendall results for variability trends are provided in Supplementary Table 3.

4. Discussion and conclusions

Our findings underscore the critical role of atmospheric dynamics in shaping MPP patterns, with far-reaching implications for ecosystem dynamics and biogeochemical cycles. They also emphasize the significant potential impacts of climate change on marine ecosystems at regional scales, as demonstrated by the persistent declining trend in CHL concentrations in the Northwestern Mediterranean Sea (Colella et al., 2016; Gómez-Jakobsen et al., 2022). This decline is driven by the steady northward shift of the JS latitudinal position. Our analysis robustly documents this trend, revealing its persistence beyond the masking effects of interannual variability. The observed decline in CHL concentrations (Fig. 11B–C and Fig. 12B, and Supp. Fig. 5B), at rates of up to −5% per year (Supp. Fig. 4), with an overall decrease of 40 %.

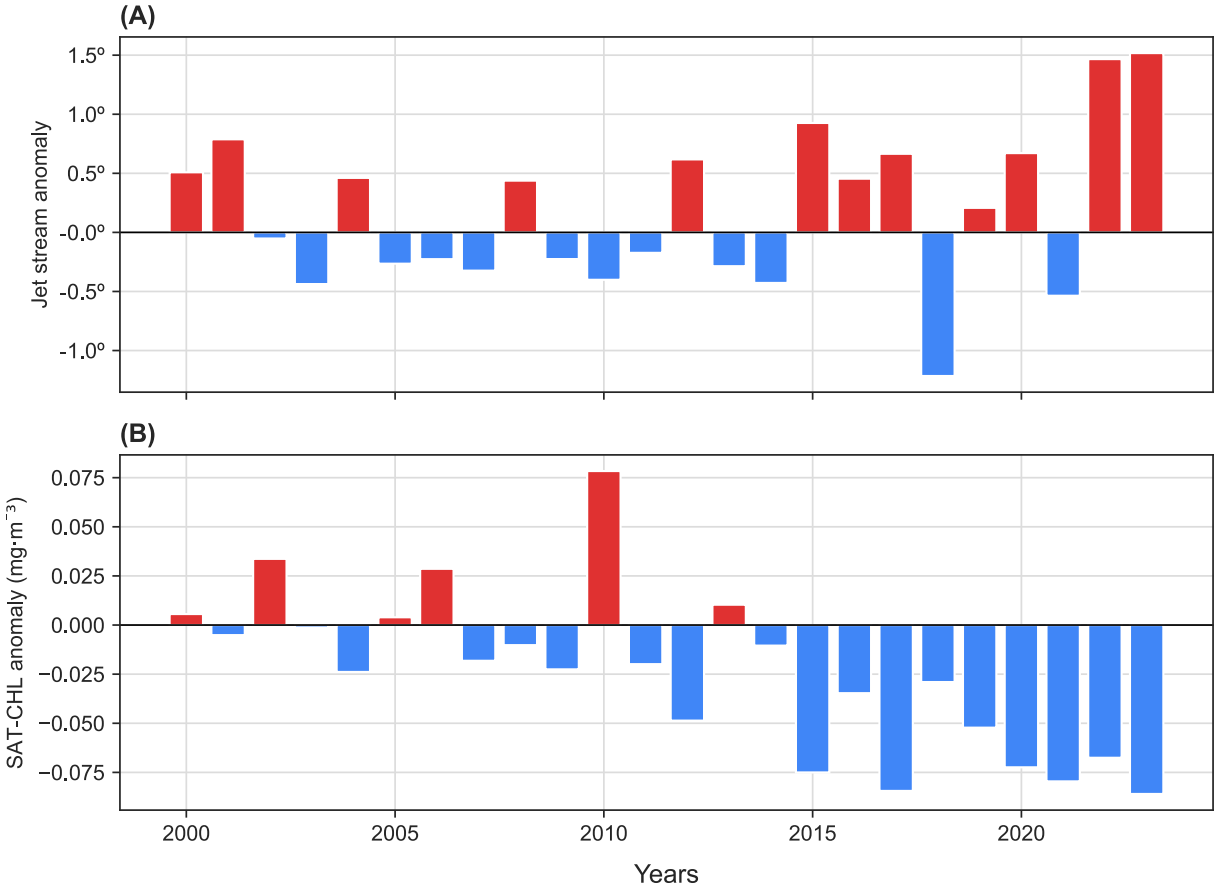

Fig. 12. Yearly anomalies relative to the reference period (2000–01-01 to 2014–12-31) of (A) Jet Stream (JS) position, and (B) surface satellite-derived chlorophyll concentration (SAT-CHL).

The mechanism driving this decline can be understood as a twofold process combining seasonal dynamics with a long-term trend. Seasonally, the typical behavior involves the northward displacement of the JS, which reduces favorable conditions for NWS and UPW (Fig. 2). This, in turn, diminishes mixing and nutrient replenishment in the surface layers of the water column, directly limiting phytoplankton productivity. However, as the JS persistently migrates poleward year after year, this seasonal mechanism translates into a cumulative, long-term reduction in CHL and MPP. Although CHL concentration is an imperfect proxy for MPP, influenced by factors such as species composition, light, and nutrient availability, it remains a widely used and consistent indicator of phytoplankton biomass. We therefore relied on satellite-derived and reanalysis CHL data, which offer direct observational coverage and temporal continuity. While model-based MPP estimates (e.g., from Copernicus products) may provide complementary insights, they often vary significantly and remain sensitive to algorithm assumptions ((Lee and Marra, 2022); Wu et al., 2024; Ryan-Keogh et al., 2023; Ryan-Keogh et al., 2025). Thus, prioritizing observed CHL data allowed us to robustly assess productivity trends in relation to JS dynamics.

Contrary to previous studies suggesting that climate change intensifies upwelling-favorable winds (Bakun, 1990; Sydeman et al., 2014; Varela et al., 2015) and that the expansion of the Azores High is enhancing coastal upwelling in the region (Rykaczewski et al., 2015; Sousa et al., 2020), our findings indicate a different trend in the EGoL subregion. Moreover, while global warming is known to intensify ocean stratification – potentially suppressing nutrient exchange and reducing upwelling effectiveness (Behrenfeld et al., 2006; Gruber, 2011; García-Reyes et al., 2015) – our results reveal a decline in upwelling events, as evidenced by the observed reduction in CHL concentration, consistent with Gómez-Jakobsen et al. (2022). This suggests that, in contrast to other marine regions where upwelling intensifies in response to atmospheric shifts, the EGoL within the Northwestern Mediterranean Sea exhibits a distinct sensitivity to JS-driven dynamics. The steady northward migration of the JS appears to be a significant driver influencing wind stress and upwelling processes, leading to a clear decline in productivity and underscoring the crucial role of JS position in shaping wind-driven oceanographic processes in the region.

Our results also emphasize that the relationship between JS position and CHL is not uniformly consistent across years. Instead, interannual variability emerges as a defining feature of this coupling, reflecting the influence of additional dynamic atmospheric and oceanographic conditions that can either reinforce or disrupt the typical JS–CHL linkage. For example, in years such as 2005 and 2012, a stronger alignment between JS and CHL is evident, suggesting atmospheric patterns that favor enhanced nutrient availability and biological response. For example, during 2012, the JS position may have favored regional conditions favourable to intense dense shelf water cascading and open-sea convection events in the Northwestern Mediterranean Sea(Durrieu De Madron et al, 2012).

However, in other years—like 2002, 2010, or 2021—this relationship weakens significantly, as shown by non-significant or even reversed correlations. These findings highlight the importance of considering short-term atmospheric anomalies, preconditioning from previous seasons, and local-scale processes (e.g., mesoscale eddies, stratification strength) that may modulate nutrient supply independent of JS-driven upwelling. We also recognize that spatial mismatches due to horizontal advection could play a role in explaining these discrepancies, with nutrient-rich waters potentially being displaced or advected away from the regions where upwelling would typically enhance productivity. Although we are unable to quantify these spatial lags in the current study, we suggest that further investigations incorporating advection velocities and current flow analysis would help resolve this complexity.

This interannual variability also reflects the inherently nonlinear and regionally specific nature of phytoplankton responses to environmental forcing. As emphasized by Salgado-Hernanz et al. (2019), phytoplankton dynamics in the region may respond to climate and environmental drivers in complex, often non-intuitive ways, depending on local oceanographic conditions and species composition. Therefore, the strength and even the direction of the JS-CHL relationship can vary across years, influenced by a variety of secondary drivers.

The similar periods observed in FFT frequencies for JS, NWS, UPW, and CHL again demonstrate the strong interdependence among these variables (Fig. 5). Moreover, the cross-correlation alignments further reinforce the idea that JS position shifts are a driving factor in CHL concentration variations, mediated through their influence on UPW dynamics, which have a faster response to JS shifts (Fig. 6). The temporal lag highlights the importance of accounting for delayed responses when analyzing the impact of atmospheric processes on marine ecosystems. Specifically, the inertial period for upwelling development at this latitude and the lag between the onset of upwelling and phytoplankton bloom formation should be carefully considered when interpreting these results. Our causality analysis by means of the convergent cross mapping causality test further supports these conclusions, demonstrating strong causal relationships between JS position and CHL, with the highest correlations observed for lags of 10–40 days in both original and deseasonalized and detrended data (Fig. 10 and Supp. Table 1). The fact that results hold across full, deseasoned, and detrended time series strengthens confidence in the observed JS–CHL relationship and suggests that this coupling is not merely a reflection of shared seasonal cycles but rather indicates a genuine dynamical linkage.

Overall, the temporal lags are consistent with the time needed for upwelling-driven nutrient supply to propagate through the food web and stimulate detectable increases in phytoplankton biomass. Previous studies have reported similar lags, typically on the order of weeks to months, depending on the ecosystem and intensity of the physical forcing (e.g., Duarte et al., 2000; Volpe et al., 2012; Chacko, 2017; Mayot et al., 2017; Basterretxea et al., 2018; Kalloniati et al., 2023). Such time scales reflect the cumulative nature of MPP responses, which involve nutrient uptake, phytoplankton growth, and biomass accumulation, all of which may blur or shift high-frequency signals observed in the physical environment.

Our findings also reveal that the JS is not only migrating northward but exhibiting increased positional variability over time, as shown by the significant positive trend in its rolling STD (Supp. Fig. 6A). This trend indicates that climate change is driving both a systematic shift and a more erratic JS behavior (Mann et al., 2017; Trouet et al., 2018), consistent with the hypothesis of a weakened, “wavier” jet stream (Stendel et al., 2021). Such increased variability can disrupt the expected cyclic forcing, leading to more unpredictable atmospheric and marine conditions on interannual timescales. Indeed, the notable concentration of JS positive anomalies in recent years suggests increasingly frequent atmospheric disruptions (Coumou and Rahmstorf, 2012; Lehmann and Coumou, 2015; Mann et al., 2017; Trouet et al., 2018) that could amplify CHL declines and further impact the marine ecosystem. Nevertheless, our study is limited in its ability to resolve the full suite of oceanic processes contributing to CHL variability. For instance, ocean currents, eddies, or mesoscale circulation patterns may redistribute productivity spatially, complicating the link between local atmospheric forcing and observed surface CHL.

While our study focuses primarily on the physical-biological coupling, the observed decline in CHL and inferred MPP may have broader implications beyond phytoplankton dynamics. In particular, long-term reductions in primary productivity could lead to cascading effects on the regional marine food web and fisheries. Similar atmospheric-forcing-driven delays in upwelling and their biological consequences have been reported in other systems, such as the California Current (Barth et al., 2007; Checkley & Barth, 2009). In the Mediterranean Sea, ecosystem modeling by Piroddi et al. (2017) identified primary productivity as the strongest environmental driver shaping biomass trends of both commercial and non-commercial species. Their findings suggest that productivity declines can propagate through trophic levels, potentially reducing fishery yields and altering food-web

structure.

In summary, while the cyclic behavior of JS-CHL interactions underscores a key driver of marine productivity, the increasing variability and erratic behavior of the JS introduces a new layer of complexity. Nonetheless, while JS position has become increasingly variable, its overall poleward shift remains a dominant and consistent driver of CHL decline in the EGoL subregion (Fig. 12B and Supp. Fig. 5B).

Our findings contribute to a deeper understanding of the complex interactions between large-scale atmospheric circulation patterns, including the upper troposphere, and marine biogeochemistry under the current climate change scenario. By elucidating the mechanisms linking JS position shifts, NWS, and UPW to MPP declines, our work highlights the vulnerability of MPP in the Northwestern Mediterranean Sea and emphasizes the importance of monitoring atmospheric forcing as a key driver of marine ecosystem changes.

However, additional in-situ observational data – particularly on nutrient concentrations, mixed layer depth, phytoplankton composition, and other MPP estimates – would be beneficial to further refine the mechanistic pathways initially proposed here. As this is one of the first studies to systematically link JS variability to CHL and MPP patterns in the Mediterranean Sea, it naturally cannot encompass the full complexity of the system. Future research using complementary methodologies, including high-resolution modeling, will be essential to build upon and expand these initial findings.

Our study underscores the need for continued multidisciplinary research to better understand atmosphere–ocean feedbacks and their effects on a variety of spatial and temporal scales. It also opens the door to future investigations, raising new questions about why JS position, NWS, UPW, and CHL exhibit stronger coupling in certain years, and exploring the underlying mechanisms that link these variables more intimately, including the role of ocean currents in transporting upwelled waters and potential bloom displacement beyond the study region.

2.1. Data

The ERA5 reanalysis products (Hersbach et al., 2023a; 2023b), available from the Copernicus Climate Change Service (C3S) through the Climate Data Store (CDS) (https://cds.climate.copernicus.eu/), were utilized in this study. These datasets provide both single-level and pressure-level data, spanning the period from 1940 to the present, with a temporal resolution of 1 h and a spatial resolution of 0.25°. For the analysis of geopotential Height (HGT), Northward Wind Stress (NWS), and Ekman pumping (UPW), we focused on 12-h data from January 1, 2000, to December 9, 2024 to maintain consistency with the other datasets used in this study.

MPP variability was assessed using daily chlorophyll concentrations, which serve as a proxy for MPP. We utilized data from the Mediterranean Sea Biogeochemistry Reanalysis dataset (Copernicus Marine Service MED-Biogeochemistry, MedBFM3 system, version 1), which has a horizontal resolution of approximately 1/24° (~4 km) (Teruzzi et al., 2021). This dataset spans from January 1, 2000, to May 31, 2023 ('MEDSEA_MULTIYEAR_BGC_006_008') (MDS, 2024).

Additionally, we incorporated daily and monthly gap-free Level-4 satellite-derived chlorophyll data from the Copernicus Marine Service multi-processing product, which has a 1 km spatial resolution. The dataset spans from January 1, 2000, to December 2, 2024 ('OCEANCOLOUR_MED_BGC_L4_MY')(MDS, 2024). These datasets provide comprehensive satellite-derived chlorophyll data across varying temporal and spatial scales, facilitating an integrated analysis of surface and depth-integrated chlorophyll data.

For the analysis of spatial trends, chlorophyll-a trend data from the Observations Reprocessing dataset ('OMI_HEALTH_CHL_MEDSEA_OCEANCOLOUR_trend') was used (MDS, 2024). This dataset, based on multi-sensor satellite observations, provides trend data covering 1997–2023.

In addition to the biogeochemical datasets, North Atlantic Oscillation (NAO) indices were obtained from the National Centers for Environmental Information (NCEI, 2024), while Western Mediterranean Oscillation (WeMO) indices (Martin-Vide and Lopez-Bustins, 2006) were accessed from the Climatic Research Unit at the University of East Anglia (Climate Research Unit, 2024).

CRediT authorship contribution statement

Júlia Crespin: Writing – review & editing, Writing – original draft, Visualization, Software, Methodology, Investigation, Formal analysis, Data curation, Conceptualization. **Jordi Solé:** Writing – review & editing, Supervision, Methodology, Investigation, Conceptualization. **Miquel Canals:** Writing – review & editing, Supervision, Investigation, Conceptualization.

Funding

JC benefits from a grant for the recruitment of researchers in training (FI-SDUR) by the Catalan Government *Generalitat de Catalunya*. CRG Marine Geosciences is funded by the Catalan Government within its excellence research groups program (ref. 2021 SGR 01195) (JC, MC). JS benefits from grant CEX2019-000928-S funded by AEI (https://doi.org/10.13039/501100011033).

Declaration of competing interest

The authors declare the following financial interests/personal relationships which may be considered as potential competing interests: [Julia Crespin reports financial support was provided by Government of Catalonia. Miquel Canals reports financial support was provided by Government of Catalonia. Jordi Sole reports was provided by Spanish State Agency of Research. If there are other authors, they declare that they have no known competing financial interests or personal relationships that could have appeared to influence the work reported in this paper].

Acknowledgments

MC acknowledges Tecnoambiente for supporting the Sustainable Blue Economy Chair of University of Barcelona. JS acknowledges Catalan Government *Generalitat de Catalunya* contract PYMEDEASCAT, *Prospectiva d'emissions a Catalunya*: pymedeascat_pro. Hersbach, H. et al., (2023a,b) were downloaded from the Copernicus Climate Change Service (2023). The results contain modified Copernicus Climate Change Service information 2020. This study has been conducted using EU Copernicus Marine Service Information doi: 10.25423/cmcc/medsea_multiyear_bgc_006_008_medbfm3, doi: 10.48670/moi-00300, and doi: 10.48670/moi-00260. Neither the European Commission nor ECMWF are responsible for any use that may be made of the Copernicus information or data it contains.

Appendix A. Supplementary data

Supplementary data to this article can be found online at https://doi.org/10.1016/j.pocean.2025.103494.

Data availability

All data used in this study are freely available in public repositories described in the paper.

References

Archer, Cristina L., Caldeira, Ken, 2008. "Historical trends in the jet streams.". Geophys. Res. Lett. 35 (8), 2008GL033614. https://doi.org/10.1029/2008GL033614.

Asiri, M.A., Almazroui, M., Awad, A.M., 2020. Synoptic features associated with the winter variability of the subtropical jet stream over Africa and the Middle East. Meteorol. Atmos. Phys. 132 (6), 819–831. https://doi.org/10.1007/s00703-019-00722-4.

Bakun, A., 1990. Global climate change and intensification of coastal ocean upwelling. Sci. 247 (4939), 198–201. https://doi.org/10.1126/science.247.4939.198.

Bakun, A., Agostini, V.N., 2001. Seasonal patterns of wind-induced upwelling/downwelling in the Mediterranean Sea. Sci. Mar. 65 (3), 243–257. https://doi.org/10.3989/scimar.2001.65n3243.

Bănaru, D., Mellon-Duval, C., Roos, D., Bigot, J.-L., Souplet, A., Jadaud, A., Beaubrun, P., Fromentin, J.-M., 2013. Trophic Structure in the Gulf of Lions Marine Ecosystem (North-Western Mediterranean Sea) and Fishing Impacts. J. Mar. Syst. 111–112, 45–68. https://doi.org/10.1016/j.jmarsys.2012.09.010.

Bane, J.M., Levine, M.D., Samelson, R.M., Haines, S.M., Meaux, M.F., Perlin, N., Kosro, P. M., Boyd, T., 2005. "Atmospheric forcing of the oregon coastal ocean during the 2001 upwelling season.". J. Geophys. Res. Oceans 110 (C10), 2004JC002653. https://doi.org/10.1029/2004JC002653.

Bane, John M., Spitz, Yvette H., Letelier, Ricardo M., Peterson, William T., 2007. "Jet stream intraseasonal oscillations drive dominant ecosystem variations in oregon's summertime coastal upwelling system.". Proc. Natl. Acad. Sci. 104 (33), 13262–13267. https://doi.org/10.1073/pnas.0700926104.

Barnes Elizabeth, A., Screen, James A., 2015. "The Impact of Arctic Warming on the Midlatitude Jet-stream: Can It? Has It? Will It?". WIREs Clim. Change 6 (3), 277–286. https://doi.org/10.1002/wcc.337.

Barth, John A., Menge, Bruce A., Lubchenco, Jane, Chan, Francis, Bane, John M., Kirincich, Anthony R., McManus, Margaret A., Nielsen, Karina J., Pierce, Stephen D., Washburn, Libe, 2007. "Delayed upwelling alters nearshore coastal ocean ecosystems in the northern California current.". Proc. Natl. Acad. Sci. 104 (10), 3719–3724. https://doi.org/10.1073/pnas.0700462104.

Basterretxea, G., Font-Muñoz, J.S., Salgado-Hernanz, P.M., Arrieta, J., Hernández-Carrasco, I., 2018. Patterns of chlorophyll interannual variability in Mediterranean biogeographical regions. Remote Sens. Environ. 215, 7–17. https://doi.org/10.1016/j.rse.2018.05.027.

Behrenfeld, M.J., O'Malley, R.T., Siegel, D.A., McClain, C.R., Sarmiento, J.L., Feldman, G.C., Milligan, A.J., Falkowski, P.G., Letelier, R.M., Boss, E.S., 2006. Climate-driven trends in contemporary ocean productivity. Nature 444 (7120), 752–755. https://doi.org/10.1038/nature05317.

Bluestein, H., 1993. Synoptic-Dynamic Meteorology in Midlatitudes: Vol II Observations and Theory of Weather Systems. In: Oxford University Press, New York, p. 594.

Canals, M., Puig, P., Madron, X.D.D., Heussner, S., Palanques, A., Fabres, J., 2006. Flushing submarine canyons. Nature 444 (7117), 354–1337. https://doi.org/10.1038/nature05271.

Chacko, N., 2017. Chlorophyll bloom in response to tropical cyclone Hudhud in the Bay of Bengal: Bio-Argo subsurface observations. Deep Sea Res. Part I 124, 66–72. https://doi.org/10.1016/j.dsr.2017.04.010.

Checkley, D.M., Barth, J.A., 2009. Patterns and processes in the California Current System. Prog. Oceanogr. 83 (1–4), 49–64. https://doi.org/10.1016/j.pocean.2009.07.028.

Climatic Research Unit, University of East Anglia. Climate Data. https://crudata.uea.ac.uk/cru/data/. (Accessed on 13-06-2024) .

Colella, S., Falcini, F., Rinaldi, E., Sammartino, M., Santoleri, R., 2016. Mediterranean ocean colour chlorophyll trends. PLoS One 11 (6), e0155756. https://doi.org/10.1371/journal.pone.0155756.

Coll, M., Bellido, J.M., Pennino, M.G., Albo-Puigserver, M., Báez, J.C., Christensen, V., Corrales, X., Fernández-Corredor, E., Giménez, J., Julià, L., Lloret-Lloret, E., Macias, D., Ouled-Cheikh, J., Ramírez, F., Sbragaglia, V., Steenbeek, J., 2024. Retrospective analysis of the pelagic ecosystem of the Western Mediterranean Sea: Drivers, changes and effects. Sci. Total Environ. 907, 167790. https://doi.org/10.1016/j.scitotenv.2023.167790.

Coumou, D., Rahmstorf, S., 2012. A decade of weather extremes. Nat. Clim. Chang. 2 (7), 491–1446. https://doi.org/10.1038/nclimate1452.

Cresswell-Clay, N., Ummenhofer, C.C., Thatcher, D.L., Wanamaker, A.D., Denniston, R. F., Asmerom, Y., Polyak, V.J., 2022. Twentieth-century Azores High expansion unprecedented in the past 1,200 years. Nat. Geosci. 15 (7), 548–553. https://doi.org/10.1038/s41561-022-00971-w.

Davis, R.E., Hayden, B.P., Gay, D.A., Phillips, W.L., Jones, G.V., 1997. The North atlantic subtropical anticyclone. J. Clim. 10 (4), 728–744. https://doi.org/10.1175/1520-0442(1997)010<0728:TNASA>2.0.CO;2.

Dawson, A., 2016. eofs: a library for EOF analysis of meteorological, oceanographic, and climate data. J. Open Res. Software 4 (1), 14. https://doi.org/10.5334/jors.122.

Dorado-Liñán, I., Ayarzagüena, B., Babst, F., Xu, G., Gil, L., Battipaglia, G., Buras, A., Čada, V., Camarero, J.J., Cavin, L., Claessens, H., Drobyshev, I., Garamszegi, B., Grabner, M., Hacket-Pain, A., Hartl, C., Hevia, A., Janda, P., Jump, A.S., Trouet, V., 2022. Jet stream position explains regional anomalies in European beech forest productivity and tree growth. Nat. Commun. 13 (1), 2015. https://doi.org/10.1038/s41467-022-29615-8.

Duarte, C., Agustí, S., Agawin, N., 2000. Response of a Mediterranean phytoplankton community to increased nutrient inputs:a mesocosm experiment. Mar. Ecol. Prog. Ser. 195, 61–70. https://doi.org/10.3354/meps195061.

Durrieu De Madron, X., L. Houpert, P. Puig, A. Sanchez-Vidal, P. Testor, A. Bosse, C. Estournel, et al. "Interaction of Dense Shelf Water Cascading and Open-sea Convection in the Northwestern Mediterranean during Winter 2012." *Geophysical Research Letters* 40, no. 7 (April 16, 2013): 1379–85. doi: 10.1002/grl.50331.

E.U. Copernicus Marine Service Information. Marine Data Store (MDS). Mediterranean Sea Biogeochemistry Reanalysis. "MEDSEA_MULTIYEAR_BGC_006_008". doi: 10.25423/cmcc/medsea_multiyear_bgc_006_008_medbfm3 (Accessed on 13-12-2024) .

E.U. Copernicus Marine Service Information. Marine Data Store (MDS). Mediterranean Sea Ocean Satellite Observations. "OCEANCOLOUR_MED_BGC_L4_MY" doi: 10.48670/moi-00300 (Accessed on 13-12-2024) .

E.U. Copernicus Marine Service Information. Marine Data Store (MDS). Mediterranean Sea Chlorophyll-a trend map from Observations Reprocessing. "OMI_HEALTH_CHL_MEDSEA_OCEANCOLOUR_trend" doi: 10.48670/moi-00260. (Accessed on 13-12-2024) .

Fedorova, N., Levit, V., Campos, A.M.V., 2018. Brazilian Northeast Jet Stream: association with synoptic-scale systems. Meteorol. Appl. 25 (2), 261–268. https://doi.org/10.1002/met.1693.

Fourrier, M., Coppola, L., D'Ortenzio, F., Migon, C., Gattuso, J., 2022. Impact of Intermittent Convection in the Northwestern Mediterranean Sea on Oxygen Content, Nutrients, and the Carbonate System. J. Geophys. Res. Oceans 127 (9), e2022JC018615. https://doi.org/10.1029/2022JC018615.

Fraysse, M., Pairaud, I., Ross, O.N., Faure, V.M., Pinazo, C., 2014. Intrusion of Rhone River diluted water into the Bay of Marseille: generation processes and impacts on ecosystem functioning. J. Geophys. Res. Oceans 119 (10), 6535–6556. https://doi.org/10.1002/2014JC010022.

García-Reyes, M., Sydeman, W.J., Schoeman, D.S., Rykaczewski, R.R., Black, B.A., Smit, A.J., Bograd, S.J., 2015. Under pressure: climate change, upwelling, and eastern boundary upwelling ecosystems. Front. Mar. Sci. 2. https://doi.org/10.3389/fmars.2015.00109.

Gómez-Jakobsen, F., Ferrera, I., Yebra, L., Mercado, J.M., 2022. Two decades of satellite surface chlorophyll a concentration (1998–2019) in the Spanish Mediterranean Marine Waters (Western Mediterranean Sea): trends, phenology and eutrophication assessment. Remote Sens. Appl.: Soc. Environ. 28, 100855. https://doi.org/10.1016/j.rsase.2022.100855.

Griffin, K.S., Martin, J.E., 2017. Synoptic features associated with temporally coherent modes of variability of the North Pacific Jet Stream. J. Clim. 30 (1), 39–54. https://doi.org/10.1175/JCLI-D-15-0833.1.

Gruber, N., 2011. Warming up, turning sour, losing breath: ocean biogeochemistry under global change. Philosophical Transactions of the Royal Society A: Mathematical, Physical and Eng. Sci. 369 (1943), 1980–1996. https://doi.org/10.1098/rsta.2011.0003.

Harris, C.R., Millman, K.J., Van Der Walt, S.J., Gommers, R., Virtanen, P., Cournapeau, D., Wieser, E., Taylor, J., Berg, S., Smith, N.J., Kern, R., Picus, M., Hoyer, S., Van Kerkwijk, M.H., Brett, M., Haldane, A., Del Río, J.F., Wiebe, M., Peterson, P., Oliphant, T.E., 2020. Array programming with NumPy. Nature 585 (7825), 357–362. https://doi.org/10.1038/s41586-020-2649-2.

Hersbach, H., Bell, B., Berrisford, P., Biavati, G., Horányi, A., Muñoz Sabater, J., Nicolas, J., Peubey, C., Radu, R., Rozum, I., Schepers, D., Simmons, A., Soci, C., Dee, D., Thépaut, J-N. (2023a): ERA5 hourly data on single levels from 1940 to present. Copernicus Climate Change Service (C3S) Climate Data Store (CDS), doi: 10.24381/cds.adbb2d47 (Accessed on 13-06-2024).

Hersbach, H., Bell, B., Berrisford, P., Biavati, G., Horányi, A., Muñoz Sabater, J., Nicolas, J., Peubey, C., Radu, R., Rozum, I., Schepers, D., Simmons, A., Soci, C., Dee, D., Thépaut, J-N. (2023b): ERA5 hourly data on pressure levels from 1940 to present. Copernicus Climate Change Service (C3S) Climate Data Store (CDS), doi: 10.24381/cds.bd0915c6 (Accessed on 13-06-2024) .

Hidalgo, M., Vasilakopoulos, P., García-Ruiz, C., Esteban, A., López-López, L., García-Gorriz, E., 2022. Resilience dynamics and productivity-driven shifts in the marine communities of the Western Mediterranean Sea. J. Anim. Ecol. 91 (2), 470–483. https://doi.org/10.1111/1365-2656.13648.

Holton, J.R., Staley, D.O., 1973. An introduction to Dynamic Meteorology. Am. J. Phys 41 (5), 752–754. https://doi.org/10.1119/1.1987371.

Hudson, R. D. "Measurements of the Movement of the Jet Streams at Mid-Latitudes, in the Northern and Southern Hemispheres, 1979 to 2010." *Atmospheric Chemistry and Physics*. 12(16) 2012 7797–7808. doi: 10.5194/acp-12-7797-2012.

Hussain, M.M., Mahmud, I., 2019. pyMannKendall: a python package for non parametric Mann Kendall family of trend tests. J. Open Source Software 4 (39), 1556. https://doi.org/10.21105/joss.01556.

Javier, P. J. E. (2021). *causal-ccm a Python implementation of Convergent Cross Mapping* (Version 0.3.3) [Github]. https://github.com/PrinceJavier/causal_ccm.

Kalloniati, K., Christou, E.D., Kournopoulou, A., Gittings, J.A., Theodorou, I., Zervoudaki, S., Raitsos, D.E., 2023. Long-term warming and human-induced plankton shifts at a coastal Eastern Mediterranean site. Sci. Rep. 13 (1), 21068. https://doi.org/10.1038/s41598-023-48254-7.

E. Kalnay, M. Kanamitsu, R. Kistler, W. Collins, D. Deaven, L. Gandin, M. Iredell, et al. "The NCEP/NCAR 40-Year Reanalysis Project." *Bulletin of the American Meteorological Society*. 77(3) 1996 437–72. doi: 10.1175/1520-0477(1996)077<0437:TNYRP>2.0.CO;2.

Katara, I., Illian, J., Pierce, G.J., Scott, B., Wang, J., 2008. Atmospheric forcing on chlorophyll concentration in the Mediterranean. Hydrobiologia 612 (1), 33–48. https://doi.org/10.1007/s10750-008-9492-z.

Keller D., Givon Y., Pennel R., Raveh-Rubin S., Drobinski P.. Untangling the Mistral and Seasonal Atmospheric Forcing Driving Deep Convection in the Gulf of Lion: 1993–2013. *Journal of Geophysical Research: Oceans*. *129*(7) 2024 e2022JC019245. doi: 10.1029/2022JC019245.

Kendall, M. G. (1970). *Rank correlation methods* (4th edition). Charles Griffin & Co Ltd, London.

Chengfeng, Le, Ming, Wu, Sun, Hongwei, Long, Shang-min, Beck, Marcus W., 2022. Linking phytoplankton variability to atmospheric blocking in an eastern boundary upwelling system. J. Geophys. Res. Oceans 127 (6), e2021JC017348. https://doi.org/10.1029/2021JC017348.

Lee, Z., Marra, J.F., 2022. The use of VGPM to estimate oceanic primary production: a "Tango" difficult to dance. J. Remote Sensing. https://doi.org/10.34133/2022/9851013.

Jascha, Lehmann, Coumou, Dim, 2015. The influence of mid-latitude storm tracks on hot, cold, dry and wet extremes. Sci. Rep. 5 (1), 17491. https://doi.org/10.1038/srep17491.

Lv, Yanmin, Jianping Guo, Jian Li, Yi Han, Hui Xu, Xiaoran Guo, Lijuan Cao, and Wenhua Gao. "Increased Turbulence in the Eurasian Upper-Level Jet Stream in Winter: Past and Future." *Earth and Space Science*. 8(2) 2021 e2020EA001556. doi: 10.1029/2020EA001556.

Macias, D., Garcia-Gorriz, E., Stips, A., 2018. Deep winter convection and phytoplankton dynamics in the NW Mediterranean Sea under present climate and future (horizon 2030) scenarios. Sci. Rep. 8 (1), 6626. https://doi.org/10.1038/s41598-018-24965-0.

Mann, H.B., 1945. Nonparametric tests against trend. Econometrica 13 (3), 245. https://doi.org/10.2307/1907187.

Mann, Michael E., Rahmstorf, Stefan, Kornhuber, Kai, Steinman, Byron A., Miller, Sonya K., Coumou, Dim, 2017. Influence of anthropogenic climate change on planetary wave resonance and extreme weather events. Sci. Rep. 7 (1), 45242. https://doi.org/10.1038/srep45242.

Many, Gaël, Ulses, Caroline, Estournel, Claude, Marsaleix, Patrick, 2021. Particulate organic carbon dynamics in the Gulf of Lion shelf (NW Mediterranean) using a coupled hydrodynamic-biogeochemical model. Biogeosciences 18 (19), 5513–5538. https://doi.org/10.5194/bg-18-5513-2021.

Martin-Vide, J., Lopez-Bustins, J.-A., 2006. The western mediterranean oscillation and rainfall in the iberian peninsula. Int. J. Climatol. 26 (11), 1455–1475. https://doi.org/10.1002/joc.1388.

Mayot, N., D'Ortenzio, F., Taillandier, V., Prieur, L., De Fommervault, O.P., Claustre, H., Bosse, A., Testor, P., Conan, P., 2017. Physical and biogeochemical controls of the phytoplankton blooms in north western mediterranean sea: a multiplatform approach over a complete annual cycle (2012–2013 DEWEX experiment). J. Geophys. Res. Oceans 122 (12), 9999–10019. https://doi.org/10.1002/2016JC012052.

Meehl, G. A., T. F. Stocker, W. D. Collins, P. Friedlingstein, A. T. Gaye, J. M. Gregory, A. Kitoh, et al. "Global Climate Projections." In *Climate Change 2007: The Physical Science Basis. Contribution of Working Group I to the Fourth Assessment Report of the Intergovernmental Panel on Climate Change*. Cambridge, United Kingdom and New York, NY, USA: Cambridge University Press, 2007. https://www.osti.gov/etdeweb/biblio/20962171.

Millot, C., 1979. Wind induced upwellings in the gulf of lions. Oceanol. Acta 2 (3), 261–274. https://archimer.ifremer.fr/doc/00122/23335/.

Millot, C., 1990. The Gulf of Lions' hydrodynamics. Cont. Shelf Res. 10 (9), 885–894. https://doi.org/10.1016/0278-4343(90)90065-T.

National Centers for Environmental Information (NCEI). North Atlantic Oscillation (NAO). https://www.ncei.noaa.gov/access/monitoring/nao/. (Accessed on 13-06-2024).

Osman, M.B., Coats, S., Das, S.B., McConnell, J.R., Chellman, N., 2021. North Atlantic jet stream projections in the context of the past 1,250 years. Proc. Natl. Acad. Sci. 118 (38), e2104105118. https://doi.org/10.1073/pnas.2104105118.

Piroddi, C., Coll, M., Liquete, C., Macias, D., Greer, K., Buszowski, J., Steenbeek, J., Danovaro, R., Christensen, V., 2017. Historical changes of the Mediterranean Sea ecosystem: modelling the role and impact of primary productivity and fisheries changes over time. Sci. Rep. 7 (1), 44491. https://doi.org/10.1038/srep44491.

Qing, Y., Wang, S., Yang, Z.-L., Gentine, P., 2023. Soil moisture–atmosphere feedbacks have triggered the shifts from drought to pluvial conditions since 1980. Commun. Earth Environ. 4 (1), 1–10. https://doi.org/10.1038/s43247-023-00922-2.

Renault, Lionel, Jacopo Chiggiato, John C. Warner, Marta Gomez, Guillermo Vizoso, and Joaquin Tintoré. "Coupled Atmosphere-ocean-wave Simulations of a Storm Event over the Gulf of Lion and Balearic Sea." *Journal of Geophysical Research: Oceans*. 117 (C9) 2012 2012JC007924. doi: 10.1029/2012JC007924.

Ryan-Keogh, T.J., Tagliabue, A., Thomalla, S.J., 2025. Global decline in net primary production underestimated by climate models. Commun. Earth Environ. 6 (1), 1–10. https://doi.org/10.1038/s43247-025-02051-4.

Ryan-Keogh, T.J., Thomalla, S.J., Chang, N., Moalusi, T., 2023. A new global oceanic multi-model net primary productivity data product. Earth Syst. Sci. Data 15 (11), 4829–4848. https://doi.org/10.5194/essd-15-4829-2023.

Rykaczewski, R.R., Dunne, J.P., Sydeman, W.J., García-Reyes, M., Black, B.A., Bograd, S. J., 2015. Poleward displacement of coastal upwelling-favorable winds in the ocean's eastern boundary currents through the 21st century. Geophys. Res. Lett. 42 (15), 6424–6431. https://doi.org/10.1002/2015GL064694.

Salgado-Hernanz, P.M., Racault, M.-F., Font-Muñoz, J.S., Basterretxea, G., 2019. Trends in phytoplankton phenology in the Mediterranean Sea based on ocean-colour remote sensing. Remote Sens. Environ. 221, 50–64. https://doi.org/10.1016/j.rse.2018.10.036.

Seabold, S., Perktold, J. (2010). *Statsmodels: Econometric and Statistical Modeling with Python*. 92–96. doi: 10.25080/Majora-92bf1922-011.

Smith, Stuart D., 1988. Coefficients for sea surface wind stress, heat flux, and wind profiles as a function of wind speed and temperature. J. Geophys. Res. Oceans 93 (C12), 15467–15472. https://doi.org/10.1029/JC093iC12p15467.

Sousa, M.C., Ribeiro, A., Des, M., Gomez-Gesteira, M., deCastro, M., Dias, J.M., 2020. NW Iberian Peninsula coastal upwelling future weakening: competition between wind intensification and surface heating. Sci. Total Environ. 703, 134808. https://doi.org/10.1016/j.scitotenv.2019.134808.

Stambler, N. (2014). The Mediterranean Sea – Primary Productivity. In: S. Goffredo, Z. Dubinsky (Eds.), *The Mediterranean Sea* (pp. 113–121). Springer Netherlands. doi: 10.1007/978-94-007-6704-1_7.

Stendel, Martin, Jennifer Francis, Rachel White, Paul D. Williams, and Tim Woollings. "The Jet Stream and Climate Change." In: *Climate Change*, 327–57. Elsevier, 2021. doi: 10.1016/B978-0-12-821575-3.00015-3.

Sugihara, G., May, R., Ye, H., Hsieh, C., Deyle, E., Fogarty, M., Munch, S., 2012. Detecting causality in complex ecosystems. Sci. 338 (6106), 496–500. https://doi.org/10.1126/science.1227079.

Sydeman, W.J., García-Reyes, M., Schoeman, D.S., Rykaczewski, R.R., Thompson, S.A., Black, B.A., Bograd, S.J., 2014. Climate change and wind intensification in coastal upwelling ecosystems. Sci. 345 (6192), 77–80. https://doi.org/10.1126/science.1251635.

Tamburini, Christian, Miquel Canals, Xavier Durrieu De Madron, Loïc Houpert, Dominique Lefèvre, Séverine Martini, Fabrizio D'Ortenzio, et al. "Deep-Sea Bioluminescence Blooms after Dense Water Formation at the Ocean Surface." Edited by John Murray Roberts. *PLoS ONE*. 8(7) 2013 e67523. doi: 10.1371/journal.pone.0067523.

Taylor, 1916. "Skin friction of the wind on the Earth's surface.". Proce. Royal Society of London. Series A, Containing Papers of a Mathematical and Physical Character 92 (637), 196–199. https://doi.org/10.1098/rspa.1916.0005.

Teruzzi, Anna, Laura Feudale, Giorgio Bolzon, Paolo Lazzari, Stefano Salon, Valeria Di Biagio, Gianluca Coidessa, and Gianpiero Cossarini. "Mediterranean Sea Biogeochemical Reanalysis (Copernicus Marine Service MED-Biogeochemistry, MedBFM3 System): MEDSEA_MULTIYEAR_BGC_006_008." 2021. doi: 10.25423/CMCC/MEDSEA_MULTIYEAR_BGC_006_008_MEDBFM3.

Touratier, F., Goyet, C., Houpert, L., Durrieu De Madron, X., Lefèvre, D., Stabholz, M., Guglielmi, V., 2016. Role of deep convection on anthropogenic CO2 sequestration in the gulf of lions (northwestern mediterranean sea). Deep Sea Res. Part I: Oceanographic Res. Papers 113, 33–48. https://doi.org/10.1016/j.dsr.2016.04.003.

Trouet, V., Babst, F., Meko, M., 2018. Recent enhanced high-summer north atlantic jet variability emerges from three-century context. Nat. Commun. 9 (1), 180. https://doi.org/10.1038/s41467-017-02699-3.

Vallis, G.K., Zurita-Gotor, P., Cairns, C., Kidston, J., 2015. Response of the large-scale structure of the atmosphere to global warming. Q. J. R. Meteorolog. Soc. 141 (690), 1479–1501. https://doi.org/10.1002/qj.2456.

Varela, R., Álvarez, I., Santos, F., deCastro, M., Gómez-Gesteira, M., 2015. Has upwelling strengthened along worldwide coasts over 1982-2010? Sci. Rep. 5 (1), 10016. https://doi.org/10.1038/srep10016.

Virtanen, P., Gommers, R., Oliphant, T.E., Haberland, M., Reddy, T., Cournapeau, D., Burovski, E., Peterson, P., Weckesser, W., Bright, J., Van Der Walt, S.J., Brett, M., Wilson, J., Millman, K.J., Mayorov, N., Nelson, A.R.J., Jones, E., Kern, R., Larson, E., Vázquez-Baeza, Y., 2020. SciPy 1.0: fundamental algorithms for scientific computing in Python. Nat. Methods 17 (3), 261–272. https://doi.org/10.1038/s41592-019-0686-2.

Volpe, G., Nardelli, B.B., Cipollini, P., Santoleri, R., Robinson, I.S., 2012. Seasonal to interannual phytoplankton response to physical processes in the Mediterranean Sea from satellite observations. Remote Sens. Environ. 117, 223–235. https://doi.org/10.1016/j.rse.2011.09.020.

Von Schuckmann, Karina, Pierre-Yves Le Traon, Neville Smith, Ananda Pascual, Samuel Djavidnia, Jean-Pierre Gattuso, Marilaure Grégoire, et al. "Copernicus Marine Service Ocean State Report, *Journal of Operational Oceanography*. 12(sup1) 2019 123. doi: 10.1080/1755876X.2019.1633075.

Wang, Dakui, Wang, Hui, Li, Ming, Liu, Guimei, Xiangyu, Wu, 2013. Role of Ekman Transport versus Ekman Pumping in Driving Summer Upwelling in the South China Sea. J. Ocean Univ. China 12 (3), 355–365. https://doi.org/10.1007/s11802-013-1904-7.

Webster, P.J., 2004. The elementary hadley circulation. In: Diaz, H.F., Bradley, R.S. (Eds.), The Hadley Circulation: Present, past and Future. Springer, Netherlands, pp. 9–60. https://doi.org/10.1007/978-1-4020-2944-8_2.

Williams, Paul D., 2016. Transatlantic flight times and climate change. Environ. Res. Lett. 11 (2), 024008. https://doi.org/10.1088/1748-9326/11/2/024008.

Woollings, Tim, Blackburn, Mike, 2012. The North Atlantic jet stream under climate change and its relation to the NAO and EA Patterns. J. Clim. 25 (3), 886–902. https://doi.org/10.1175/JCLI-D-11-00087.1.

Woollings, T., Hannachi, A., Hoskins, B., 2010. Variability of the North Atlantic Eddy-Driven Jet Stream: Variability of the North Atlantic Jet Stream. Q. J. R. Meteorolog. Soc. 136 (649), 856–868. https://doi.org/10.1002/qj.625.

Woollings, T., Drouard, M., O'Reilly, C.H., Sexton, D.M.H., McSweeney, C., 2023. Trends in the atmospheric jet streams are emerging in observations and could be linked to tropical warming. Commun. Earth Environ. 4 (1), 1–8. https://doi.org/10.1038/s43247-023-00792-8.

Wu, J., Lee, Z., Goes, J., do R.Gomes, H., Wei, J., 2024. Evaluation of three contrasting models in estimating primary production from ocean color remote sensing using long-term time-series data at oceanic and coastal sites. Remote Sens. Environ. 302, 113983. https://doi.org/10.1016/j.rse.2023.113983.

Xu, G., Broadman, E., Dorado-Liñán, I., Klippel, L., Meko, M., Büntgen, U., De Mil, T., Esper, J., Gunnarson, B., Hartl, C., Krusic, P.J., Linderholm, H.W., Ljungqvist, F.C., Ludlow, F., Panayotov, M., Seim, A., Wilson, R., Zamora-Reyes, D., Trouet, V., 2024. Jet stream controls on European climate and agriculture since 1300 ce. Nature 634 (8034), 600–608. https://doi.org/10.1038/s41586-024-07985-x.

Ye, H., Deyle, E.R., Gilarranz, L.J., Sugihara, G., 2015. Distinguishing time-delayed causal interactions using convergent cross mapping. Sci. Rep. 5 (1), 14750. https://doi.org/10.1038/srep14750.